Article

SOURCE DATA | TRANSPARENT PROCESS

EMBO reports

The coordination of spindle-positioning forces during the asymmetric division of the *Caenorhabditis elegans* zygote

Hélène Bouvrais[1,*], Laurent Chesneau[1], Yann Le Cunff[1], Danielle Fairbrass[1], Nina Soler[1], Sylvain Pastezeur[1], Thierry Pécot[2], Charles Kervrann[2] & Jacques Pécréaux[1,**]

Abstract

In *Caenorhabditis elegans* zygote, astral microtubules generate forces essential to position the mitotic spindle, by pushing against and pulling from the cortex. Measuring microtubule dynamics there, we revealed the presence of two populations, corresponding to pulling and pushing events. It offers a unique opportunity to study, under physiological conditions, the variations of both spindle-positioning forces along space and time. We propose a threefold control of pulling force, by polarity, spindle position and mitotic progression. We showed that the sole anteroposterior asymmetry in dynein on-rate, encoding pulling force imbalance, is sufficient to cause posterior spindle displacement. The positional regulation, reflecting the number of microtubule contacts in the posterior-most region, reinforces this imbalance only in late anaphase. Furthermore, we exhibited the first direct proof that dynein processivity increases along mitosis. It reflects the temporal control of pulling forces, which strengthens at anaphase onset following mitotic progression and independently from chromatid separation. In contrast, the pushing force remains constant and symmetric and contributes to maintaining the spindle at the cell centre during metaphase.

Keywords force coordination; microtubule dynamics; polarity control; spindle-positioning; temporal control

Subject Categories Cell Adhesion, Polarity & Cytoskeleton; Cell Cycle

DOI 10.15252/embr.202050770 | Received 29 April 2020 | Revised 22 February 2021 | Accepted 3 March 2021 | Published online 26 April 2021

EMBO Reports (2021) 22: e50770

Introduction

During asymmetric division, the position of the mitotic spindle is accurately regulated. Its final position participates in the correct partition of cell fate determinants, which is crucial to ensure faithful division during developmental processes (Gönczy, 2008; Neumüller & Knoblich, 2009; Morin & Bellaïche, 2011; McNally, 2013; Kotak, 2019). Furthermore, its position at the late metaphase controls the pulling force burst (Bouvrais *et al,* 2018). In the one-cell embryo of the nematode *Caenorhabditis elegans*, the mitotic spindle is first oriented along the polarity axis and positioned at the cell centre. Then, the spindle is maintained at that position for a few minutes during metaphase. Finally, it is displaced towards the posterior before division (Gönczy, 2008; McNally, 2013). So far, cell-scale investigations revealed the forces at the core of this precise choreography but remained elusive in their regulation. In particular, force generators pull on astral microtubules from the cell periphery, corresponding to the cell cortex and cause the posterior displacement. The force generators are composed of the dynein/dynactin complex, the LIN-5^{NuMA} protein and the G-protein regulators GPR-1/2^{LGN} and are anchored at the membrane through Gα subunits (Gotta & Ahringer, 2001; Colombo *et al,* 2003; Srinivasan *et al,* 2003; Couwenbergs *et al,* 2007; Nguyen-Ngoc *et al,* 2007). This trimeric complex generates forces through dynein acting as molecular motor and/or tracking the plus-end of depolymerising microtubule (Schmidt *et al,* 2005; Kozlowski *et al,* 2007; Nguyen-Ngoc *et al,* 2007; O'Rourke *et al,* 2010; Laan *et al,* 2012a). Opposite to this cortical pulling, the centring force maintains the spindle at the cell centre during metaphase. Its mechanism is still debated with three major possibilities (Wühr *et al,* 2009; Wu *et al,* 2017): specific regulation of the cortical pulling forces (Tsou *et al,* 2002; Grill & Hyman, 2005; Kimura & Onami, 2007; Gusnowski & Srayko, 2011; Laan *et al,* 2012a); pulling forces generated by dynein localised at cytoplasmic organelles (Kimura & Onami, 2005; Kimura & Kimura, 2011; Shinar *et al,* 2011; Barbosa *et al,* 2017); and cortical pushing forces resulting from the growing of astral microtubules against the cortex (Garzon-Coral *et al,* 2016; Pécréaux *et al,* 2016), similarly to the mechanism found in yeast (Tran *et al,* 2001; Tolic-Nørrelykke *et al,* 2004). So far, these studies were all based on cell-scale measurements.

How are the cortical pulling and pushing forces regulated and coordinated in space and time? The previous studies approached them separately, resorting to spatial or temporal averages. The cortical pulling forces are asymmetric, because of a higher number

1 CNRS, IGDR - UMR 6290, University of Rennes, Rennes, France
2 INRIA, Centre Rennes - Bretagne Atlantique, Rennes, France
*Corresponding author. Tel: +33 2 23 23 40 08; E-mail: helene.bouvrais@univ-rennes1.fr
**Corresponding author. Tel: +33 2 23 23 45 03; E-mail: jacques.pecreaux@univ-rennes1.fr

of *active* force generators—trimeric complexes engaged in pulling events with astral microtubules—at the posterior-most region of the embryo (Gotta *et al,* 2003; Grill *et al,* 2003; Pécréaux *et al,* 2006a; Nguyen-Ngoc *et al,* 2007; Rodriguez-Garcia *et al,* 2018), in response to polarity cues (Grill *et al,* 2001; Colombo *et al,* 2003; Tsou *et al,* 2003; Park & Rose, 2008; Krueger *et al,* 2010; Bouvrais *et al,* 2018). Besides, the physical basis of the progressive increase in the pulling force along the course of the division was inferred from cell-scale measurements, particularly during anaphase, and a molecular mechanism is still missing (Labbé *et al,* 2004; Pécréaux *et al,* 2006a; Campbell *et al,* 2009; Bouvrais *et al,* 2018). Furthermore, the spatiotemporal regulation of the centring force is still unknown, as well as its coordination with opposed pulling force. We here addressed this gap, through analysing the astral microtubules contacting the cortex.

Astral microtubules are involved in generating all these forces. These semi-flexible filaments emanate from the spindle poles. They are dynamic, switching alternatively from growing to shrinking and back, at the catastrophe and rescue rates, respectively (Mitchison & Kirschner, 1984). At the cortex, astral microtubules can be in three different states: shrinking in coordination with cortex-anchored dynein that generates pulling force (Gonczy *et al,* 1999; Dujardin & Vallee, 2002; Grishchuk *et al,* 2005; Gusnowski & Srayko, 2011; Laan *et al,* 2012a; Rodriguez-Garcia *et al,* 2018); pushing by growing against the cortex, likely helped by stabilising associated proteins like CLASP (Faivre-Moskalenko & Dogterom, 2002; Dogterom *et al,* 2005; Howard, 2006; Espiritu *et al,* 2012); or stalled, clamped possibly by dynein tethering or other proteins (Labbé *et al,* 2003; Sugioka *et al,* 2018). Do the microtubule dynamics, especially their cortical residence times, reflect these different states? Interestingly, dynein tethering delays microtubule catastrophe, as shown *in vitro* and by computational studies (Hendricks Adam *et al,* 2012; Laan *et al,* 2012a). Oppositely, the larger the pushing force, the smaller the residence time (Janson *et al,* 2003). In *C. elegans* embryo, microtubules involved in pulling or pushing forces may display different cortical residence times (Pécréaux *et al,* 2006a; Pécréaux *et al,* 2016). They could thus reveal the corresponding force-generating events. For instance, previous studies uncovered anteroposterior variations in residence time. The microtubules would be more dynamic (lower lifetime) at the posterior cortex compared to the anterior (Labbé *et al,* 2003; Sugioka *et al,* 2018). However, the reported residence times are strikingly different between studies (Labbé *et al,* 2003; Kozlowski *et al,* 2007; O'Rourke *et al,* 2010; Hyenne *et al,* 2012; Schmidt *et al,* 2017; Sugioka *et al,* 2018). How the microtubule residence times evolve throughout mitosis is, however, yet to be studied. Indeed, the short duration of these cortical fluorescent spots of labelled microtubules (a few frames) and the low signal-to-noise ratio of the images made resolving both time and space variations hard until now. Recent developments in microscopy and image-processing tools call for revisiting this problem (Chenouard *et al,* 2014; Kervrann *et al,* 2016).

Beyond imaging improvements, the statistical analysis of the durations of microtubule tracks at the cortex—resulting from following the same fluorescent spots over several images—could also be significantly refined in contrast to the classic fit with a mono-exponential distribution (Kozlowski *et al,* 2007; Sugioka *et al,* 2018). In particular, we here aim to distinguish several co-existing dynamical behaviours. Thus, we fitted the experimental distribution of the track durations with finite-mixture-of-exponential models and then used an objective criterion to choose the best one. Such an approach, although delicate, benefits from developments in applied mathematics (Grinvald & Steinberg, 1974; James & Ware, 1985; Vieland & Hodge, 1998; Jae Myung *et al,* 2000; Turton *et al,* 2003). Furthermore, in our case, the microtubule residence times could last only a few tenths of a second, i.e. a few frames. The discrete nature of the residence time histogram calls for specific analysis as performed in photon counting experiments. This field has designed appropriate fitting strategies that offer a firm starting point to analyse microtubule dynamics (Maus *et al,* 2001; Turton *et al,* 2003; Nishimura & Tamura, 2005; Laurence & Chromy, 2010).

In the present paper, we aim to study the spatiotemporal regulation of the spindle-positioning forces during the first mitotic division of the *C. elegans* embryo. To do so, we measured the microtubule dynamics at the cell periphery. We designed the *DiLiPop assay* (Distinct Lifetime subPopulation) to disentangle several microtubule populations distinct by their cortical residence times. We found two of them, which we could associate with different microtubule functions. Equipped with this assay, we could investigate in time and space, and at the microscopic level, the regulation of the forces positioning the spindle during mitosis. We directly measured the force generator processivity increase that accounts for the pulling force regulation throughout mitosis. We showed that the three controls of pulling force (by polarity, spindle position and mitotic progression) act independently. We also identified which mechanism maintains the spindle at the cell centre during metaphase. Finally, we suggest how the two cortical forces, pushing and pulling, coordinate in space and time.

Results

The Distinct Lifetime (sub)Population (DiLiPop) assay reveals two populations of microtubules at the cortex

To investigate the regulation of the forces exerted on the mitotic spindle during the first mitosis of the *C. elegans* zygote, we set to measure the dynamics of astral microtubules at the cortex. The microtubules were entirely fluorescently labelled using YFP::α-tubulin to view them in all their states. The thickness of the perivitelline space, about 250–500 nm, prevented the use of the TIRF microscopy without altering the embryo shape (Olson *et al,* 2012). We performed spinning disc microscopy at the cortical plane, at 10 frames per second similarly to Bouvrais *et al,* (2018) (Appendix Text §1.1.1). The high frame rate needed to resolve the brief cortical contacts led to images with a low signal-to-noise ratio (Fig 1A, top). We mitigated this issue by denoising using the Kalman filter (Fig 1A, middle; Movie EV1, right) (Kalman, 1960). However, we did not correct any bleaching to avoid artefact, preferring to work out the imaging conditions. We then tracked the microtubule contacts using the u-track algorithm (Fig 1A, bottom; Appendix Table S1; Appendix Text §1.1.2) (Jaqaman *et al,* 2008). This image-processing pipeline is further named *KUT*. During metaphase and anaphase, the microtubule tracks appeared as fluorescent spots, suggesting that the microtubules did not slide or bend along the cortex (Movie EV1). The tracks were classified mainly as diffusive-like, based on the asymmetry in the position scatter along each

trajectory (Huet *et al,* 2006; Jaqaman *et al,* 2008). Besides, each microtubule visited a limited cortical region (< 1 μm^2 in average, Appendix Text §1.1.2), in agreement with microtubule end-on cortical-interaction (Laan *et al,* 2012a). We estimated that it enabled us to capture at least 2/3 of the microtubule contacts (Appendix Fig S1A) by comparing with electron tomography (Redemann *et al,* 2017).

To ensure that fluorescent spots were associated with microtubule contacting the cortex and not with free tubulin in the cytoplasm, we permeabilised embryos by *perm-1(RNAi)* and performed a nocodazole treatment as in (Carvalho *et al,* 2011) (Appendix Fig S2A) (Appendix Text §1.1.3). After microtubule depolymerisation, we obtained a negligible number of tracks at the cortex, about 1 or 2 per frame, which was ten to forty times less than in untreated embryos (Appendix Fig S2B). The control embryos treated with DMSO appeared similar to non-treated. It confirmed that the tracks studied here corresponded to astral microtubules contacting the cortex. We furthermore computed the count of instantaneous contacts in untreated embryos. They increased around anaphase onset (Appendix Fig S1A) similarly to the microtubule dynamics (Srayko *et al,* 2005). They also increased with the centrosome approaching the cortex (Bouvrais *et al,* 2018) (Appendix Text §1.1.3). Importantly, the instantaneous count of microtubule contacts at the posterior cortex oscillated during anaphase as in (Kozlowski *et al,* 2007). The period was comparable to the one of the posterior centrosome oscillation. These oscillations depended on GPR-1/2 (Appendix Fig S3) (Appendix Text §1.1.3). We overall concluded that the investigated spots corresponded to astral microtubules reaching the cortex.

We computed the duration distributions of the microtubule tracks for each embryo separately (to avoid averaging artefacts) (Fig 1B). When all the microtubules have the same catastrophe rate, this distribution follows an exponential decay (Kozlowski *et al,* 2007; Floyd *et al,* 2010). However, we also envisaged that multiple mechanisms are superimposed, leading to distinct catastrophe rates. Therefore, we fitted the duration distribution with finite-mixture-of-exponential models, in particular, double- and triple-exponential models (Appendix Text §1.2.1). The double exponential appeared to fit better, suggesting that we observed at least two populations of microtubules contacting the cortex of *C. elegans* embryo, distinct by their residence times (Fig 1C). These populations might offer the opportunity to visualise the various force-generating mechanisms. To finely characterise them, we implemented an advanced statistical analysis of the track-duration distribution (Fig 1D), described in details in Appendix Text §1.2. In a nutshell, because we fitted a histogram with few counts in some bins, we modelled the data point errors using a Poisson law. We designed the objective function correspondingly to fit the histogram (Fig 1D, grey shading) (Appendix Text §1.2.2) (Laurence & Chromy, 2010). To distinguish between multiple populations within each embryo from a single population per cell with parameters varying between embryos, we fitted each embryo individually. However, to gain certainty, we imposed the same model parameters on each embryo of a given data set, by global fitting, i.e. maximising the product of the embryo-wise likelihoods (Fig 1D, green) (Appendix Text §1.2.3) (Beechem, 1992). We performed an unbiased selection of the best mixture-of-exponential model using the Bayesian Inference Criterion (*BIC*) (Fig 1D, blue) (Appendix Text §1.2.4) (Schwarz, 1978). Finally, we computed the confidence intervals on the fitted parameters using bootstrapping (Fig 1D, purple; Appendix Fig S1D) (Appendix Text §1.2.5) (Efron & Tibshirani, 1993). We validated this approach using the likelihood ratio (Appendix Fig S1E) (Bolker, 2008; Agresti, 2013). Applying this approach to untreated embryos of *C. elegans*, we found two populations within the microtubules residing at the cortex (Fig 1EF, Appendix Table S2). Their distinct dynamics, whose lifetimes were in the range of the second, were in agreement with residence time measurements performed with high enough image acquisition rate (Kozlowski *et al,* 2007; O'Rourke *et al,* 2010; Lacroix *et al,* 2016; Schmidt *et al,* 2017; Sugioka *et al,* 2018). It suggested that the microtubules could be involved in two different mechanisms. In contrast, performing the DiLiPop assay on embryos treated with nocodazole, we found a very-short-lived population, whose lifetime was briefer than the short-lived one, and no long-lived population (Appendix Fig S2C). Control embryos (DMSO) showed a two-population behaviour similar to non-treated ones (Appendix Fig S2C compared to Fig 1F). Therefore, the few remaining tracks upon nocodazole treatment corresponded likely to detection noise (Appendix Text §1.1.3). In conclusion, our analysis reflected astral microtubule dynamics out of the noise.

We firstly asked how dependent on imaging conditions were the results (Appendix Text §1.1.4). We applied our DiLiPop analysis to untreated α-tubulin-labelled embryos acquired at 20 Hz and compared the result to our untreated embryo data set, comprising 25 embryos acquired at 10 Hz. We observed fewer tracks due to the reduced sensitivity linked to the shorter exposure time (Appendix Fig S4A). However, we found two populations with lifetimes similar to the reference data set ones (Appendix Fig S4B). We performed a converse analysis and simulated a 2 frames per second acquisition through a running sum of 5 images on our reference data set. We obtained fewer tracks, since those below 0.5 s were not resolved (Appendix Fig S4C). The recovered-tracks analysis resulted in a single population with a lifetime close to the long-lived one measured at 10 Hz (Appendix Fig S4D). In conclusion, our results were independent of the frame rate provided it is fast enough to resolve the short-lived population.

We secondly ensured that our complex pipeline could not create the two dynamically distinct populations through artefacts. We built images containing particles with a single dynamical behaviour (Appendix Fig S5A, black; Appendix Table S3; Materials and Methods) (Costantino *et al,* 2005). By DiLiPop analysis, we recovered a single population with the correct lifetime (Appendix Fig S5A, red). In contrast, a similar simulation with two dynamical populations led to the double exponential as the best model (Appendix Fig S5B, blue) and accurate lifetimes (Appendix Fig S5B, right). Overall, the KUT image-processing pipeline did not cause artefacts. However, and to gain certainty, we repeated the analysis of *in vivo* data using an image-processing pipeline based on different hypotheses. This pipeline, named *NAM*, encompasses the ND-SAFIR denoising (Appendix Fig S6B, middle) (Boulanger *et al,* 2010), the ATLAS spot-detecting (Basset *et al,* 2015) and the MHT linking (Multiple Hypothesis Tracker) (Appendix Fig S6B, right) (Chenouard *et al,* 2013), with settings listed in Appendix Table S4 (Appendix Text §1.1.5). Applied to untreated *C. elegans* embryos, the NAM pipeline combined to DiLiPop statistical analysis recovered the two populations distinct by their dynamics (Appendix Fig S6A, green). Furthermore, the lifetimes were close to the ones obtained using the KUT

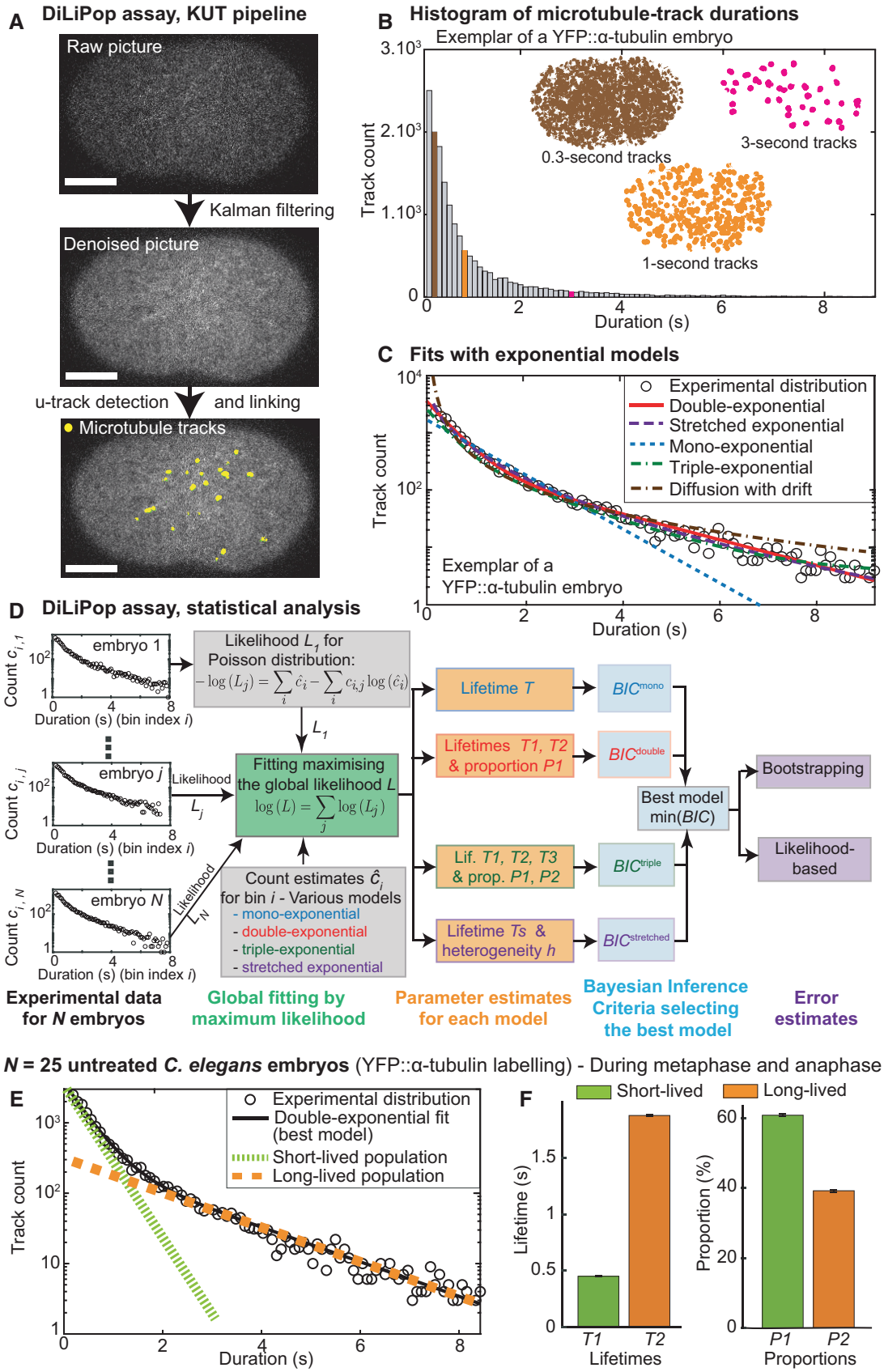

Figure 1.

Figure 1. Microtubule dynamics at the cortex of the *Caenorhabditis elegans* embryo encompass two distinct residence time behaviours during the first zygotic division.

The typical workflow of the DiLiPop (Distinct Lifetime subPopulation) assay disentangles microtubule populations.

A (Top) Bright spots are the plus-ends of the fluorescently labelled microtubules. (Middle) Spots are enhanced after denoising by a Kalman filter. (Bottom) The trajectories of the microtubules (yellow lines) are obtained using the u-track algorithm (Appendix Text, §1.1.2). The parameters used are in Appendix Table S1. Scale bar represents 10 μm.

B Experimental distribution of the microtubule track durations for an embryo imaged from nuclear envelope breakdown to late anaphase. (Insets) Spatial distributions of the tracks lasting 0.3 s (brown), 1 s (orange) and 3 s (pink).

C The above experimental distribution (open circles) was fitted using various exponential models: (dashed blue line) mono-exponential, (plain red line) double exponential, (dash-dotted green line) triple-exponential, (dashed purple line) stretched exponential and (dash-dotted brown line) a diffusion with drift model (Appendix Text, §1.2.1). The double exponential model was the most satisfactory visually. This was confirmed applying the approach described in (D).

D Flow diagram of the advanced statistical analysis used in the DiLiPop assay (Appendix Text, §1.2). (White boxes) Exemplar distributions (histograms), depicting the count $c_{i,j}$ per duration-bin (indexed by i), j indexing the embryo. (Grey shadings) The experimental distributions of the microtubule track durations for N embryos were individually fitted using different exponential models (Appendix Text, §1.2.1) and assuming a Poisson distribution (Appendix Text, §1.2.2). (Green shading) We maximised the global likelihood L, computed as the product of embryo likelihoods L_j (Appendix Text, §1.2.3). (Orange shadings) We thus obtained the model parameters for each studied model. (Blue shadings) The best model was selected as the one minimising the Bayesian Inference Criterion (*BIC*) (Appendix Text, §1.2.4). (Purple shadings) We estimated the standard deviations on the best model parameters by using either a bootstrap approach (Appendix Fig S1D) or the likelihood-based confidence intervals (Appendix Fig S1E) (Appendix Text, §1.2.5).

E Microtubule track durations of $N = 25$ untreated embryos (same condition as in (B, C)) were subjected to DiLiPop global fit. The best-fitting model was the double exponential (black line). Dotted green and dashed orange lines highlight the separate contributions of each exponential component, respectively, short- and long-lived. The *BIC* values for each model are reproduced in Appendix Table S2.

F Corresponding fit parameters and error bars, which are standard deviations (SD) obtained by bootstrapping.

Data information: Imaging of YFP::α-tubulin-labelled embryos was performed at a frame acquisition rate of 10 Hz. KUT and statistical analyses are illustrated with a one-cell untreated embryo. The data set composed of $N = 25$ untreated *C. elegans* embryos is also used in the Figs 2A, 4A and B, and 6A, in Appendix Figs S1A, S4, S6C and D, S12A and B, and S14 and Appendix Table S2.
Source data are available online for this figure.

pipeline (Appendix Fig S6A, right). We, therefore, excluded that the two dynamically distinct populations could be artifactual.

We estimated that we analysed about 2/3 of the microtubule contacts at the cortex compared to the theoretical expected ones. While this proportion was high, we wondered whether the remaining 1/3 could correspond to a particular population. Firstly, we reused the fabricated images containing particles displaying two dynamical behaviours and compared the recovered population-proportion with the assigned one. Both proportions were similar. Therefore, our KUT pipeline introduced no bias analysing fabricated images (Appendix Fig S5B, right). Secondly, to investigate this point on real images, we compared the recovered proportions obtained through the KUT and NAM analysis pipelines applied to untreated embryos. We observed similar populations, both in lifetimes and proportions (Appendix Fig S6A, right), which suggested again that viewing 2/3 of expected microtubules introduced no bias. Furthermore, the similarity of the results obtained using two pipelines different by their approaches made unlikely that the remaining 1/3 of contacts would correspond to an additional population.

Along a similar line and before investigating the biological relevance of these populations, we wondered whether there might be even more than two populations in general. We reasoned that the number of data points, typically ~20,000 microtubule tracks per embryo, may be insufficient to support a triple-exponential model. We addressed this question *in silico* and simulated distributions of microtubule track durations creating "*simulated embryos*", with three dynamical populations of lifetimes 0.4, 1.5 and 4 s, and proportions set to 55, 40 and 5%, respectively. These values correspond to experimental estimates on untreated embryos (Appendix Table S2). To mimic the experimental conditions of untreated embryos, we generated "*fabricated datasets*" composed of 25 simulated embryos and analysed them using the DiLiPop assay. We repeated 10 times this simulation procedure to get certainty about the results. We further considered only the sample sizes, for which a majority of fabricated data sets led to the simulated model, here triple-exponential, being the best model according to Bayesian criterion. Among valid conditions, we averaged the recovered model parameters over the data sets, where the recovered best model was correct. It suggested that 20,000 tracks per embryo were necessary and also sufficient to support the triple-exponential model if applicable (Appendix Fig S7A). We reckoned that a third and very-long-lived population might be in such a low proportion that the amount of experimental data did not allow identifying it. Keeping with our *in silico* approach and using 20,000 tracks per embryo, we fixed the short-lived proportion to 55% and the very-long-lived one from 2.5 to 10%. We found that 5% was enough to support the triple-exponential model (Appendix Fig S7B). We concluded that in untreated embryos, there is less than 5% or no very-long-lived population of astral microtubules.

Being confident in the biological origin of the two microtubule populations, we wondered whether two well-defined microtubule populations exist or whether the numerous molecular motors and microtubule-associated proteins (MAPs) could lead to a broadly-varying microtubule residence time. We modelled this latter case using a stretched exponential (Lee *et al,* 2001; Siegel *et al,* 2001). Such a model was not the best, analysing untreated embryos (Appendix Table S2). However, we again asked whether the amount of experimental data was sufficient, using *in silico* approach. We simulated microtubule durations displaying a stretched exponential behaviour of lifetime 0.1 s and heterogeneity parameter 2.2, which were the experimental estimates on untreated embryos (Appendix Table S2). We found that 500 tracks per embryo were sufficient (Appendix Fig S7C). Because we had far more tracks in experimental data, we ascertained that the stretched exponential model was not suitable. We then wondered whether the detected spots could correspond to short microtubules nucleated near the cortex. A

microtubule growing in the imaging plane will be detected above a threshold length l_{min}. We expected the lifetime to follow the distribution of first passage times for a microtubule of length l_{min} to return to that length after having grown longer, assuming the microtubule length followed a bias random walk (Bicout, 1997; Needleman *et al,* 2010). We fitted the experimental distribution using a power law with an exponential cut-off (Appendix Text §1.2.1). However, such a model did not adjust well the experimental duration distribution and was not selected by the Bayesian inference criterion (Fig 1C, Appendix Table S2). Therefore, the investigated fluorescent spots were unlikely to reflect microtubule nucleation close to the cortex. We concluded that the two dynamical behaviours measured *in vivo* truly correspond to two populations of microtubules.

Being assured that we observed microtubules, likely astral, contacting the cortex, we asked whether it reflects the force-generating events. Alternatively, the labelling or variations in the dosage of tubulin paralogs within the microtubules could account for our observations (Wright & Hunter, 2003; Honda *et al,* 2017). As an alternative to the labelling used above, YFP::TBA-2$^{\alpha\text{-tubulin}}$, we repeated our experiment using GFP::TBB-2$^{\beta\text{-tubulin}}$ (Appendix Fig S6C) and measured two populations of microtubules at the cortex, with similar lifetimes (Appendix Fig S6C, right). The change in lifetimes was noticeable for the long-lived population and could originate from distinct dye-brightness or sensitivity to bleaching. These differences are comparable to the ones observed when changing the image-processing pipeline (Appendix Text §1.1.5). We concluded that the two microtubule populations are likely to reflect distinct force-generating events.

Finally, we wondered whether such two microtubule populations exist beyond *C. elegans*. We investigated the microtubule dynamics at the cortex in a cousin nematode species, *Caenorhabditis briggsae*, where β-tubulin was labelled. We again observed two populations distinct by their dynamics (Appendix Fig S6D). We concluded that these two populations are not a peculiarity of *C. elegans* embryo. Overall, by viewing the microtubule contacts in all their states, we measured two populations at the cortex. Because they are dynamically distinct, a possible interpretation was that they reflected pulling and pushing force-generating events. Indeed, pushing microtubules are likely to reside longer to contribute to centring (Garzon-Coral *et al,* 2016; Pécréaux *et al,* 2016; Howard & Garzon-Coral, 2017), while short residence times could correspond to events of pulling by dynein, proposed to last about 0.5 s (Pécréaux *et al,* 2006a; Rodriguez-Garcia *et al,* 2018).

The short- and long-lived microtubules correspond to events of pulling from and pushing against the cortex

More dynein engaged in pulling on the posterior side causes the cortical pulling force imbalance and the spindle posterior displacement during the anaphase of the asymmetric division of the nematode zygote (Grill *et al,* 2003; Redemann *et al,* 2010; Rodriguez-Garcia *et al,* 2018). We reckoned that it might be reflected in an uneven distribution of short-lived and long-lived contacts. We refined the DiLiPop assay to map the cortical contacts along the anteroposterior axis (AP axis) within each population. We selected biologically relevant regions and time-blocks as small as possible, yet guaranteeing enough data to detect two populations accurately (Appendix Text §1.3, Appendix Fig S8). We applied this analysis to untreated embryos and recovered the high contact density ridgelines, for both populations, as previously reported (Bouvrais *et al,* 2018) (Fig 2A). About 50 s before the anaphase onset, the instantaneous contact density of the short-lived population increased posteriorly and became asymmetric (Fig 2A, left). The short-lived microtubules were particularly enriched in the region where the force generators are active and which extends from 70 to 100% along the AP axis (Krueger *et al,* 2010; Bouvrais *et al,* 2018). In contrast, the long-lived contact density remained symmetric, with a slight posterior enrichment in late anaphase, expected because the spindle displaces towards the posterior (Fig 2A, right) (Bouvrais *et al,* 2018). The specific polarisation of the short-lived population suggested that the corresponding microtubule contacts revealed pulling force-generating events.

To further support this result, we genetically decreased or increased cortical pulling forces and observed the spatial distribution of the short-lived microtubule density (Rodriguez-Garcia *et al,* 2018). Firstly, we depleted GPR-1/2^{LGN}, the well-established force generator regulator (Colombo *et al,* 2003; Grill *et al,* 2003; Pécréaux *et al,* 2006a; Nguyen-Ngoc *et al,* 2007). We used *gpr-2(ok1179)* mutant embryos with *gpr-1/2(RNAi)* treatment to ensure a strong depletion and computed the DiLiPop-map. We observed a significant reduction in the short-lived microtubule density in the posterior-most region compared to the control during anaphase (Fig 2BC). It led to cancelling out the asymmetric distribution of this population. In similar conditions, we imaged at the spindle plane and tracked the spindle poles in $N = 8$ embryos. We observed a loss of spindle pole oscillation and a strong reduction of the spindle posterior displacement as reported previously (Colombo *et al,* 2003; Pécréaux *et al,* 2006a) (Appendix Fig S10D). Since the short-lived-population distribution strongly depends on GPR-1/2, the corresponding microtubules are likely to contribute to generate pulling force.

Secondly, we performed the converse experiment, enriching the force generators anteriorly through a *cnsk-1(RNAi)* treatment (Panbianco *et al,* 2008). We observed a significant increase in the short-lived microtubule density anteriorly, compared to controls (Fig 2BC), consistent with previous observation using labelled dynein (Rodriguez-Garcia *et al,* 2018). We also observed a slight decrease in the short-lived densities at the posterior-most region attributed to the anterior displacement of the spindle (Appendix Fig S10D) (Bouvrais *et al,* 2018; Rodriguez-Garcia *et al,* 2018). Under the same conditions and at the spindle plane, we observed a clear increase in centrosome oscillation amplitudes anteriorly 4.0 ± 0.2 μm ($N = 11$ embryos) compared to 2.2 ± 0.1 μm in control embryos (two-tailed Student's *t*-test: $P = 9{\times}10^{-3}$, $N = 7$ control embryos). We also measured slightly increased oscillations at the posterior pole, although not significantly, with peak-to-peak amplitude of 5.4 ± 0.1 μm compared to 5.1 ± 0.2 μm (two-tailed Student's *t*-test: $P = 0.62$). It confirmed the significant increase in pulling forces mostly at anterior (Panbianco *et al,* 2008). Overall, the short-lived microtubule density correlates with both the cortical force intensity and the number of active force generators, supporting our interpretation of the short-lived population.

We reckoned that the long-lived population might then correspond to microtubules pushing against the cortex. To challenge this idea, we impaired microtubule growth by moderately depleting the promoting factor ZYG-9^{XMAP215} by RNAi. We then performed a

DiLiPop analysis during metaphase without splitting into regions to gain accuracy and since the long-lived population is not polarised. We recovered more than 2,500 tracks per embryo, neatly enough to quantify two populations during metaphase with 8 embryos (Appendix Fig S9A and E, light-brown arrows; Appendix Text §2). We found two populations, but interestingly, only the long-lived

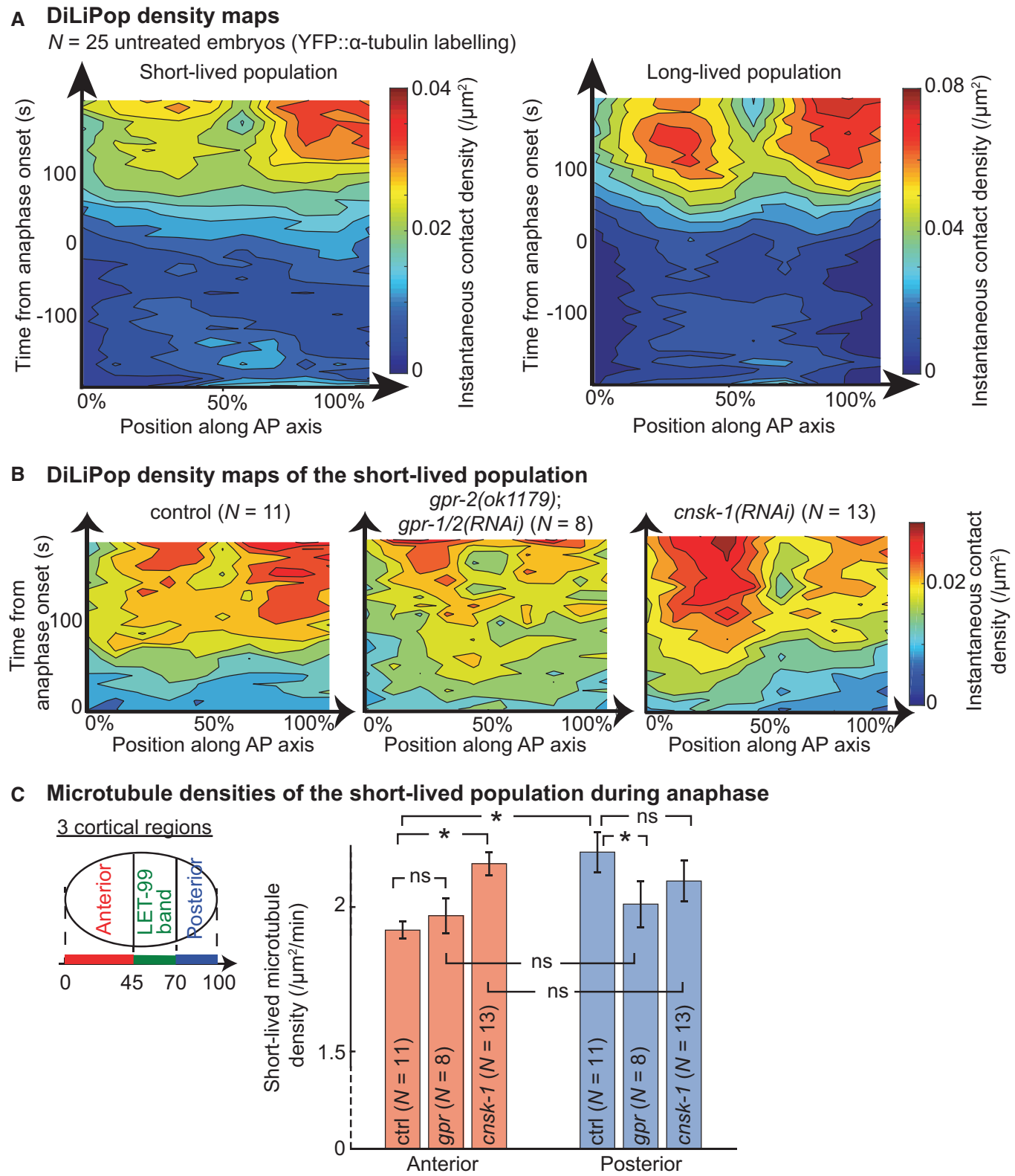

Figure 2.

Figure 2. Microtubules pulling from the cortex belong to the short-lived population.

A DiLiPop density maps, computed for a data set of $N = 25$ untreated α-tubulin-labelled embryos, show the instantaneous distributions of (left) the short-lived and (right) the long-lived contacts along the anteroposterior axis (AP axis), during metaphase and anaphase. The DiLiPop mapping attributes each contact to a population (Appendix Text, §1.3). We used 3 regions and 60-s time-blocks. The heat map is computed by averaging the mapped contacts within 10 regions of equal width along the AP axis and over a 10-s running window for each embryo. These maps were then averaged over the data set (Appendix Text, §1.3).

B Short-lived-contact density maps of (left) $N = 11$ control embryos, (middle) $N = 8$ *gpr-2(ok1179);gpr-1/2(RNAi)*-treated embryos and (right) $N = 13$ *cnsk-1(RNAi)*-treated embryos. To determine the characteristics of the two populations, we used 3 regions and the whole anaphase.

C Corresponding comparisons of the short-lived microtubule densities in the anterior region (0 - 45% of AP axis, red) and posterior-most region (70 - 100% of AP axis, blue). For concision, *gpr* stands for *gpr-2(ok1179);gpr-1/2(RNAi)*.

Data information: In (C), error bars are SD obtained by bootstrapping (Appendix Text, §1.2.5). Star indicates significant differences (Student's *t*-test; *, $P \leq 0.01$). In (A), the data set composed of $N = 25$ untreated *C. elegans* embryos is also used in the Figs 1E and F, 4A and B, and 6A, in Appendix Figs S1A, S4, S6C and D, S12A and B, S14 and Appendix Table S2. The data set composed of *cnsk-1(RNAi)*-treated embryos is also used in the Appendix Fig S10, and the one composed of *gpr-2(ok1179);gpr-1/2(RNAi)*-treated embryos in Fig EV2 and Appendix Fig S10.
Source data are available online for this figure.

microtubules had their lifetime significantly reduced while the short-lived one was unaltered (Fig 3A, green). It was consistent with the reported activity of ZYG-9 (Bellanger & Gönczy, 2003; Srayko *et al,* 2003; Brouhard *et al,* 2008). It supported our hypothesis that the long-lived population accounts for pushing microtubules. Under the same conditions and at the spindle plane, we observed a reduction of the metaphase spindle length before elongation, which reads 8.7 ± 0.7 μm upon *zyg-9(RNAi)* ($N = 8$) compared to 10.2 ± 0.9 μm in control embryos (Student's *t*-test: $P = 3.7 \times 10^{-3}$, $N = 7$), as expected (Srayko *et al,* 2003). To strengthen the link between the long-lived population and the growing microtubules, we partially depleted the microtubule-depolymerising kinesin KLP-7^{MCAK} by a hypomorphic RNAi treatment. The DiLiPop analysis revealed no significant change in the lifetime of the long-lived population during metaphase (Fig 3A left, blue). We also found that the short-lived population displayed a slightly increased residence time (Fig 3A right, blue) consistent with the increased pulling forces previously reported (Grill *et al,* 2001; Gigant *et al,* 2017). When imaging at the spindle plane during anaphase, we measured a faster spindle elongation equal to 0.156 ± 0.020 μm/s upon *klp-7(RNAi)* ($N = 9$) compared to 0.102 ± 0.026 μm/s for the control embryos (Student's *t*-test: $P = 1.8 \times 10^{-5}$, $N = 13$), as expected (Grill *et al,* 2001; Gigant *et al,* 2017). We concluded that the long-lived population reflects specifically microtubule growing against the cortex, leading to pushing force.

To better distinguish the two populations, we set to label specifically the growing microtubules using an EBP-2::GFP strain as previously done (Kozlowski *et al,* 2007). We found a single microtubule population with a lifetime intermediate between the two obtained using YFP::α-tubulin labelling (Fig 3B). On the one hand, we could attribute this result to a direct effect of EBP-2 over-expression, which would alter microtubule dynamics, as seen in other organisms (Duellberg *et al,* 2016). On the other hand, the microtubule can reside at the cortex and push against it with a reduced GTP cap resulting in a loss of EBP-2::GFP signal but not YFP::α-tubulin one (Fig 3C). Indeed, *in vitro* experiments found a delay between the cap disappearing and catastrophe (Bieling *et al,* 2007; Kozlowski *et al,* 2007; Zanic *et al,* 2009). Furthermore, proteins like CLASP or even dynein can stabilise the microtubule (Espiritu *et al,* 2012; Laan *et al,* 2012b). In a broader take, we suggested that the long-lived population reflects specifically microtubules pushing against the cortex (Fig 3D, orange). Meanwhile, perturbations of cortical pulling force level or distribution are visible on the short-lived microtubules, relating these latter to the pulling force-generating events (Fig 3D, green).

The asymmetric dynein on-rate sets the final spindle position independently from positional control and mitotic progression

Multiple mechanisms regulating the cortical pulling forces were proposed. Monitoring them through DiLiPop offered an unparalleled opportunity to investigate the links between these controls, termed polarity, positional and temporal (mitotic progression). Indeed, others and we suggested that mitotic progression acts through regulating force generator off-rate, the inverse of the processivity, i.e. the persistence of the force generators to pull on microtubule before detaching (Labbé *et al,* 2004; Pécréaux *et al,* 2006a; McCarthy Campbell *et al,* 2009; Bouvrais *et al,* 2018). We also proposed that a higher dynein-microtubule on-rate at the posterior cortex, compared to the anterior one, causes the cortical pulling force imbalance. It reflects the polarity and accounts for the spindle posterior displacement (Fielmich *et al,* 2018; Rodriguez-Garcia *et al,* 2018). This on-rate could be the binding rate of force generator dynein to the microtubules or its engaging rate, i.e. the initiation of a motor run to exert a pulling force. Concurrently, we also reported the regulation of these same forces by the position of the spindle itself (Bouvrais *et al,* 2018).

We firstly investigated the link between polarity and temporal control. To do so, we compared the anterior (0-45% of AP axis) and posterior-most (70-100% of AP axis) regions over time, using, in particular, the Wilcoxon signed-rank test. We measured the short-lived population since it corresponds to the pulling force. We observed that the asymmetry in the short-lived microtubule density existed all along mitosis (Fig 4A and B, left) in contrast to the lifetime that remained mostly symmetric (Fig 4A and B, right). It showed that pulling force imbalance exists from at least late metaphase. The posterior-to-anterior ratio of densities agreed with the one of spindle pole velocity after spindle cut (Grill *et al,* 2001; Nguyen-Ngoc *et al,* 2007; Schmidt *et al,* 2017; Fielmich *et al,* 2018; Sugioka *et al,* 2018). The characteristics of the short-lived population were also consistent with dyneins being denser on posterior but persisting same times on both sides (Rodriguez-Garcia *et al,* 2018). It may suggest that force polarisation is independent of the mitotic progression.

To further explore the link between these two controls, we treated either wild-type embryos by RNAi against *lin-5*, or *gpr-2 (ok1179)* mutant embryos by RNAi against *gpr-1/2*, to symmetrise

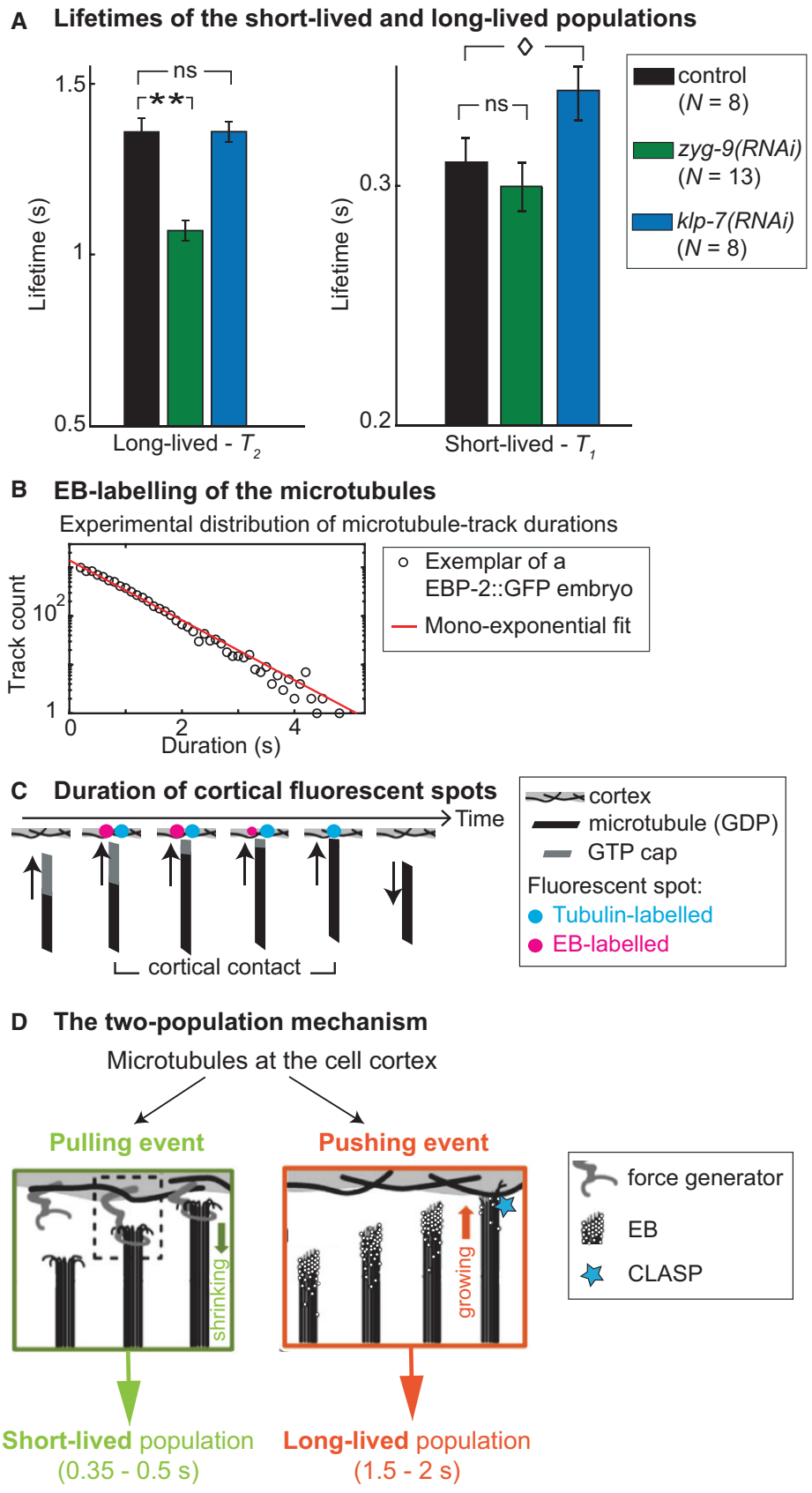
A Lifetimes of the short-lived and long-lived populations
ns
**
ns
◇
1.5
1
0.5
0.3
0.2
Lifetime (s)
Long-lived - T_2
Short-lived - T_1
control (N = 8)
zyg-9(RNAi) (N = 13)
klp-7(RNAi) (N = 8)
B EB-labelling of the microtubules
Experimental distribution of microtubule-track durations
Track count
10^2
1
0
2
4
Duration (s)
Exemplar of a EBP-2::GFP embryo
Mono-exponential fit
C Duration of cortical fluorescent spots
Time
cortical contact
cortex
microtubule (GDP)
GTP cap
Fluorescent spot:
Tubulin-labelled
EB-labelled
D The two-population mechanism
Microtubules at the cell cortex
Pulling event
Pushing event
shrinking
growing
force generator
EB
CLASP
Short-lived population
(0.35 - 0.5 s)
Long-lived population
(1.5 - 2 s)

Figure 3.

Figure 3. The microtubules pushing against the cortex belong to the long-lived population.

A DiLiPop analysis of the microtubule dynamics at the cortex during metaphase, in (green) $N = 13$ *zyg-9(RNAi)*-treated embryos, (blue) $N = 8$ *klp-7(RNAi)*-treated embryos, and (black) $N = 8$ control embryos. We compared the lifetimes of (left) the long-lived and (right) the short-lived populations.

B Experimental distribution of the microtubule track-durations for a typical EB-labelled embryo. Over $N = 9$ embryos, the distributions were best fitted by a mono-exponential, with a lifetime equal to 0.64 s.

C Schematic highlighting the putative mechanism causing different cortical residence times upon (pink) EB- and (blue) tubulin-labellings.

D The two-population mechanism: the short-lived microtubules account for pulling force-generating events, while the long-lived ones for pushing force-generating events.

Data information: In (A), error bars are SD obtained by bootstrapping (Appendix Text, §1.2.5). Stars or diamond indicate significant differences (Student's *t*-test; $*P \leq 0.05$; $**P \leq 0.001$).
Source data are available online for this figure.

the pulling dynein density. We observed that the short-lived density of microtubules became symmetric upon both treatments (Fig EV1A and B; Appendix Fig S10A and B). Interestingly, the lifetimes of the short-lived population were not affected, indicating that the reduction of force imbalance was likely independent of the control of processivity, i.e. mitotic progression (Fig EV2A and B). To strengthen our hypothesis, we treated embryos using *goa-1;gpa-16 (RNAi)*. This protein is also involved in cortical pulling force and may anchor the trimeric complex (Gotta & Ahringer, 2001; Afshar *et al,* 2004; Afshar *et al,* 2005; Park & Rose, 2008). We observed, as expected, a reduced asymmetry of the short-lived densities (Fig EV1A and B). The short-lived microtubule lifetimes upon *goa-1;gpa-16(RNAi)* were similar to control ones (Fig EV2B). In the same conditions, at the spindle plane, we observed a reduced spindle posterior displacement and a suppression of oscillations in these 3 conditions (Appendix Fig S10D, Fig EV1C). The effect was however milder for *lin-5(RNAi)* and *goa-1;gpa-16(RNAi)*. On the one hand, *lin-5(RNAi)* treatment was hypomorphic, because the corresponding protein is involved in earlier processes (van der Voet *et al,* 2009); on the other hand, *RNAi* targeting two genes, *goa-1* and *gpa-16*, is knowingly less efficient. In conclusion, it indicated that the mitotic progression control through force generator processivity acts independently from polarity control through GPR-1/2 posterior enrichment and dynein on-rate.

We reckoned that the regulation of microtubule cortical residence times could be separated from the trimeric complex, but still under the control of polarity proteins PAR-2 and PAR-3 (Labbé *et al,* 2003; Sugioka *et al,* 2018). As expected, *par-3(RNAi)* and *par-2 (RNAi)* treatments resulted in a reduction in the density asymmetry of the short-lived-population (Fig 5A, Appendix Fig S11A) accounting for the centred final spindle position (Appendix Fig S11B). Indeed, the asymmetric distribution of GPR-1/2 is PAR-dependent (Gotta & Ahringer, 2001; Colombo *et al,* 2003; Gotta *et al,* 2003; Srinivasan *et al,* 2003; Tsou *et al,* 2003; Pécréaux *et al,* 2006a; Fielmich *et al,* 2018; Rodriguez-Garcia *et al,* 2018). Importantly, it did not affect the mitotic progression, suggesting this latter control may be independent of the force generator density. Indeed, in both depletions, we observed a strong increase in the lifetimes of the short-lived and long-lived populations (Fig 5B and C), consistent with pulling force increase along mitosis. However, all cortical regions were equally affected, maintaining the anteroposterior symmetry of the lifetimes in treated and control conditions. It further showed that the force generator processivity does not encode the pulling force imbalance. Overall, we suggest that the polarity and mitotic progression controls act independently, respectively, through the dynein on-rate (density of active force generators) and dynein off-rate (their processivity). Furthermore, PAR-2 and PAR-3 proteins play an additional role in globally scaling, likely indirectly, microtubule residence times at the cortex.

We next asked whether the microtubules could push against the cortex asymmetrically and displace the spindle posteriorly. Indeed, such a mechanism was proposed and modelled in other organisms (Pavin *et al,* 2012; Zhao *et al,* 2012). To test this possibility, we investigated the temporal evolution of the long-lived-population parameters using 60-s time-blocks. We measured symmetric densities until mid-anaphase (Appendix Fig S12A and B, left). The lifetimes in anterior and posterior-most regions were quite similar. They were larger anteriorly only in late anaphase (Appendix Fig S12A and B, right). Because this asymmetry happened later than the spindle posterior displacement, it suggested that microtubule growing may not contribute to the causative force imbalance.

To gain certainty, we increased the force due to pushing microtubules. EFA-6^{PSD} was reported to negatively regulate both dynein-dependent pulling force generator and cortical microtubule stability (O'Rourke *et al,* 2007; O'Rourke *et al,* 2010). The DiLiPop analysis of *efa-6(RNAi)*-treated embryos showed a modest increase in the short-lived microtubule density (Fig EV3A and B) and a stronger increase in the long-lived one (Fig EV3A and C). In the same condition at the spindle plane, we observed reduced peak-to-peak oscillation amplitudes for the posterior centrosome (2.33 ± 1.60 μm, $N = 11$) compared to control embryos (5.11 ± 0.90 μm, Student's *t*-test: $P = 2.5 \times 10^{-4}$, $N = 8$), as expected (O'Rourke *et al,* 2010). Importantly, we only observed a slightly increased posterior displacement of the posterior centrosome, however non-significant (Fig EV3D). It contrasted with the large increase of the long-lived microtubule density and suggested that microtubule pushing is unlikely to contribute to the posterior displacement. We recently suggested that it maintains the spindle at the cell centre instead (Pécréaux *et al,* 2016).

We next investigated hypothetical links between the positional control and the polarity one. We recently proposed that a scarcity of microtubule contacts in the posterior-most region reduced the dynein on-rate and thus pulling forces. Indeed, during metaphase, the spindle is centred and the centrosomes are far from embryo tips (Krueger *et al,* 2010; Bouvrais *et al,* 2018). The spindle moves towards the posterior from late metaphase to anaphase. Both long-lived and short-lived populations undergo such a geometrical effect thought to increase the number of contacts, while polarity control affects only the short-lived microtubules. We thus measured the density of long-lived microtubules and observed an asymmetry only

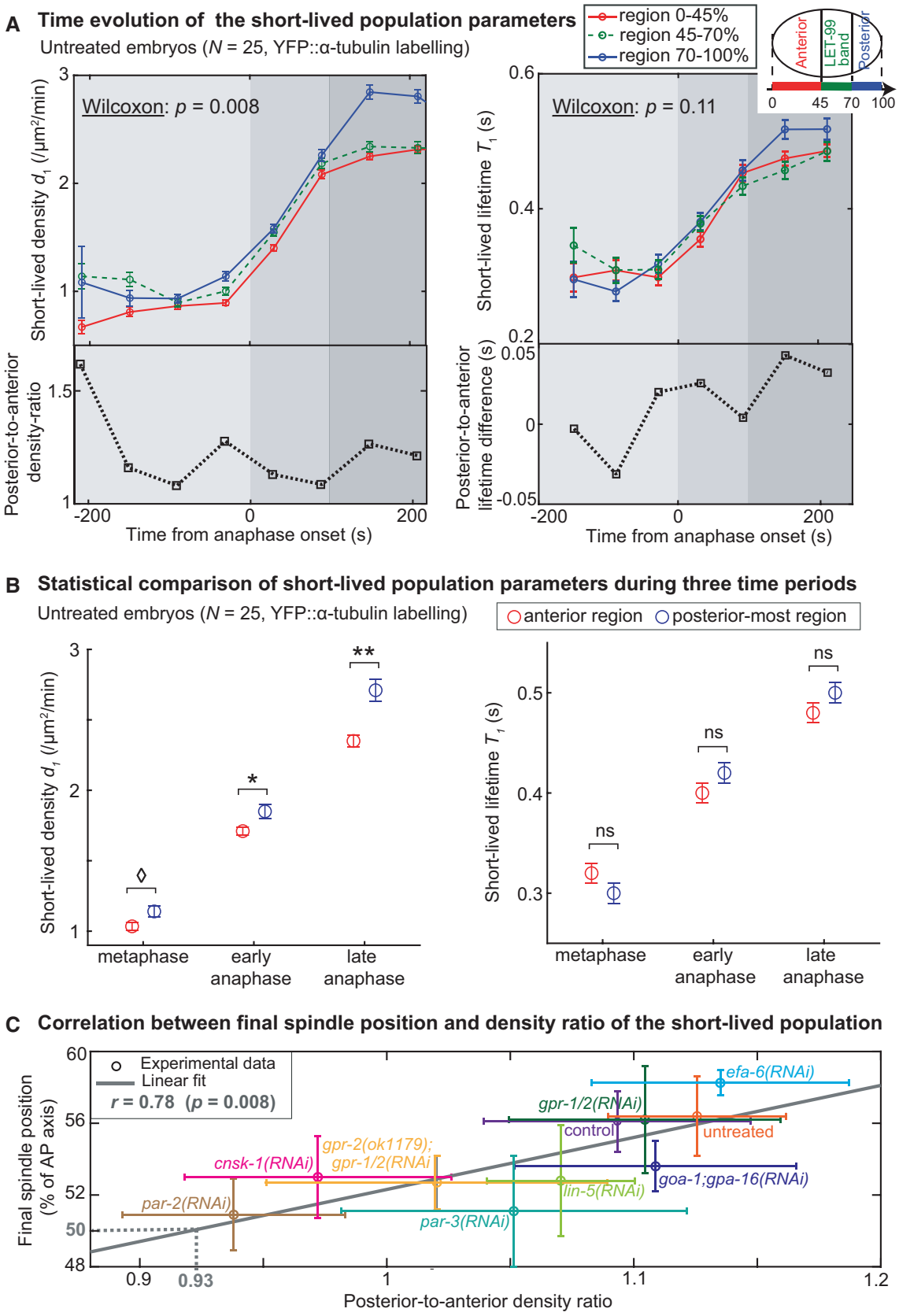
A
Time evolution of the short-lived population parameters
Untreated embryos (N = 25, YFP::α-tubulin labelling)
region 0-45%
region 45-70%
region 70-100%
Anterior
LET-99 band
Posterior
0
45
70
100
Wilcoxon: p = 0.008
Short-lived density d1 (/µm²/min)
Posterior-to-anterior density-ratio
Time from anaphase onset (s)
Wilcoxon: p = 0.11
Short-lived lifetime T1 (s)
Posterior-to-anterior lifetime difference (s)
Time from anaphase onset (s)
B
Statistical comparison of short-lived population parameters during three time periods
Untreated embryos (N = 25, YFP::α-tubulin labelling)
anterior region
posterior-most region
Short-lived density d1 (/µm²/min)
metaphase
early anaphase
late anaphase
Short-lived lifetime T1 (s)
ns
C
Correlation between final spindle position and density ratio of the short-lived population
Experimental data
Linear fit
r = 0.78 (p = 0.008)
Final spindle position (% of AP axis)
Posterior-to-anterior density ratio
efa-6(RNAi)
gpr-1/2(RNAi)
control
untreated
gpr-2(ok1179); gpr-1/2(RNAi
cnsk-1(RNAi)
goa-1;gpa-16(RNAi)
lin-5(RNAi)
par-2(RNAi)
par-3(RNAi)
0.93

Figure 4.

Figure 4. An asymmetry in the short-lived microtubule density ratio is sufficient to cause the posterior displacement of the spindle.

A Evolution of the short-lived population parameters of $N = 25$ untreated α-tubulin-labelled embryos, during metaphase and anaphase: (top left) microtubule densities and (top right) lifetimes, in (red) the anterior region, (green) the lateral LET-99 band and (blue) the posterior-most region. These regions are depicted in the schematics at the top right. We used 60-s time-blocks. Below each plot, either (left) the posterior-to-anterior density ratio or (right) the posterior-to-anterior lifetime difference is plotted. We found a significant difference between the time-series of anterior and posterior-most regions for the densities, as supported by the Wilcoxon signed-rank test, but not for the lifetimes. The grey shadings depict, from lighter to darker, the three time periods, namely metaphase (the 210 s before anaphase onset), early anaphase (the 100 s after anaphase onset) and late anaphase (from 100 s to 210 s after anaphase onset).

B We analysed the same quantities as (A) comparing the two extreme regions and reducing the time resolution to the three time periods for the sake of accuracy.

C Final spindle position obtained by imaging the same strain at the spindle plane plotted against the posterior-to-anterior density ratio for the short-lived population, assessed during the whole anaphase. The grey line depicts the Pearson correlation ($r = 0.78$, χ^2 test $P = 0.008$). The density ratio varied by depleting various proteins: *par-3(RNAi)* ($N = 10$ embryos acquired at the cortex and $N = 12$ at the spindle plane, further written 10/12), *par-2(RNAi)* ($N = 9/14$), *gpr-2(ok1179);gpr-1/2(RNAi)* ($N = 8/8$), *cnsk-1(RNAi)* ($N = 13/9$), *lin-5(RNAi)* ($N = 13/14$), *goa-1;gpa16(RNAi)* ($N = 12/9$), *gpr-1/2(RNAi)* ($N = 11/6$), *efa-6(RNAi)* ($N = 10/11$), control embryos $N = 11/10$ and untreated embryos $N = 25/9$. Error bars are the standard deviations. The dotted grey line indicates the short-lived density ratio for a centred final position of the spindle, estimated from the linear regression.

Data information: Error bars are SD obtained (A, B, C X-axis) by bootstrapping (Appendix Text, §1.2.5) or (C Y-axis) from raw data. In (B), stars or diamond indicate significant differences (Student's *t*-test; $\diamond P \leq 0.05$; $^*P \leq 0.01$; $^{**}P \leq 0.001$). In (A, B), the data set composed of $N = 25$ untreated *C. elegans* embryos is also used in the Figs 1E and F, 2A, and 6A, in Appendix Figs S1A, S4, S6C and D, S12A and B, S14 and Appendix Table S2.
Source data are available online for this figure.

in late anaphase (Appendix Fig S12A and B, left). At that time, the spindle already migrated posteriorly. Therefore, the positional control merely reinforces the posterior displacement lately but does not cause it.

To gain certainty about the role of this positional control, we used again CNSK-1 depletion to alter polarity. Consistently, the time-resolved measurement of short-lived microtubule density showed no significant asymmetry but a slight anterior enrichment in metaphase (Appendix Fig S10A right, S10B left). Importantly, we measured a global upscaling of the long-lived densities, but no alteration of their spatial distribution in comparison to the control (Appendix Fig S10C). The spindle was displaced anteriorly in this treatment (Appendix Fig S10D), and we expected both populations to be equally affected through the positional control. But *cnsk-1(RNAi)* altered only the balance of regional densities for the short-lived population. Therefore, the polarity regulation appeared sufficient to account for the spindle displacement out of the cell centre. We concluded that positional and polarity controls are independent. Again, the positional control can reinforce the asymmetry later in anaphase.

Lastly, to ascertain that the sole asymmetry of dynein density, due to its on-rate, accounts for force imbalance, we asked whether the final position of the spindle correlated with the posterior short-lived-population enrichment. We tested the correlation of this position and the posterior-to-anterior density ratio of the two populations, during anaphase (Materials and Methods). We obtained a more pronounced correlation for the short-lived microtubules (Fig 4C, Appendix Fig S12C). Interestingly, the spindle-centred position was estimated by linear regression to correspond to a ratio equal to 0.93 for the short-lived population (Fig 4C, dotted grey line)—an almost symmetric distribution. In a broader take, we concluded that the pulling force imbalance is recapitulated by the asymmetric density ratio of the short-lived population. In turn, this density corresponded to the binding rate of dynein to microtubule or its run initiation.

The mitotic progression controls the force generator processivity

The cortical pulling force increases during mitosis (Labbé *et al,* 2004; McCarthy Campbell *et al,* 2009). In our modelling of pulling force, we attributed it to the increasing processivity of the force generator, lately reinforced by the positional control (Pécréaux *et al,* 2006a; Bouvrais *et al,* 2018). Since the dynein processivity is reflected in the short-lived microtubule lifetime in our assay, the DiLiPop offers an opportunity to validate the mechanism of pulling force increase, at the microscopic scale. We measured the temporal evolution of the two lifetimes using 30-s time-blocks but not distinguishing various regions to gain certainty and because we excluded that lifetimes contributed to the force imbalance. We found a steep increase in the short-lived microtubule lifetime during the early anaphase, continued by a shallower one in late anaphase (Fig 6A, left). In contrast, the lifetime remained constant during metaphase. Such a variation accounted for the force measured at cell scale. However, we also observed the same increase-pattern for the long-lived population (Fig 6A, right) although the variation amplitude was reduced, especially considering relative values. Importantly, both time-series were likely independent during metaphase (Pearson: $r = 0.73$, χ^2 test $P = 0.098$). It may suggest a specific regulation of the lifetime of the short-lived population, which would superimpose to a general regulation visible on both populations.

We sought a condition perturbing the lifetime of one of the two populations, to test such a regulation difference. We depleted the microtubule rescue factor CLS-2$^{\mathrm{CLASP}}$. It is expected to affect astral microtubule quite independently of cortical pulling force generators (Srayko *et al,* 2005; Espiritu *et al,* 2012). We kept the *cls-2(RNAi)* treatment hypomorphic to ensure functional metaphasic or central spindle (Cheeseman *et al,* 2005; Maton *et al,* 2015). We observed a different evolution of short- and long-lived microtubule lifetimes during late anaphase (Fig EV4A). We also found a significant reduction in the long-lived microtubule lifetime after mid-anaphase, while the short-lived lifetime was only slightly downscaled (Fig EV4C). Furthermore, while the short-lived times-series of *cls-2(RNAi)*-treated and control embryos were correlated, the long-lived ones were mildly independent (Fig EV4A and B). It suggested that CLS-2 depletion affected mostly the long-lived population. Under the same condition and at the spindle plane, we measured a faster spindle elongation equal to 0.517 ± 0.287 μm/s upon *cls-2(RNAi)* (Student's *t*-test: $P = 9.8 \times 10^{-4}$, $N = 10$) compared to 0.083 ± 0.027 μm/s for the control embryos ($N = 7$), confirming the penetrance of the RNAi

treatment (Espiritu *et al*, 2012). Because CLS-2 is a probable rescue factor, it was relevant that pushing force-related microtubules were especially affected. In all case, it suggested that the lifetimes may be differentially regulated between both populations.

We next sought an alteration of the spindle position not impairing pulling force regulation. Indeed, it could reveal whether the two lifetimes are separately regulated. We set to reduce the spindle to a single centrosome (or two centrosomes not clearly separated) performing a

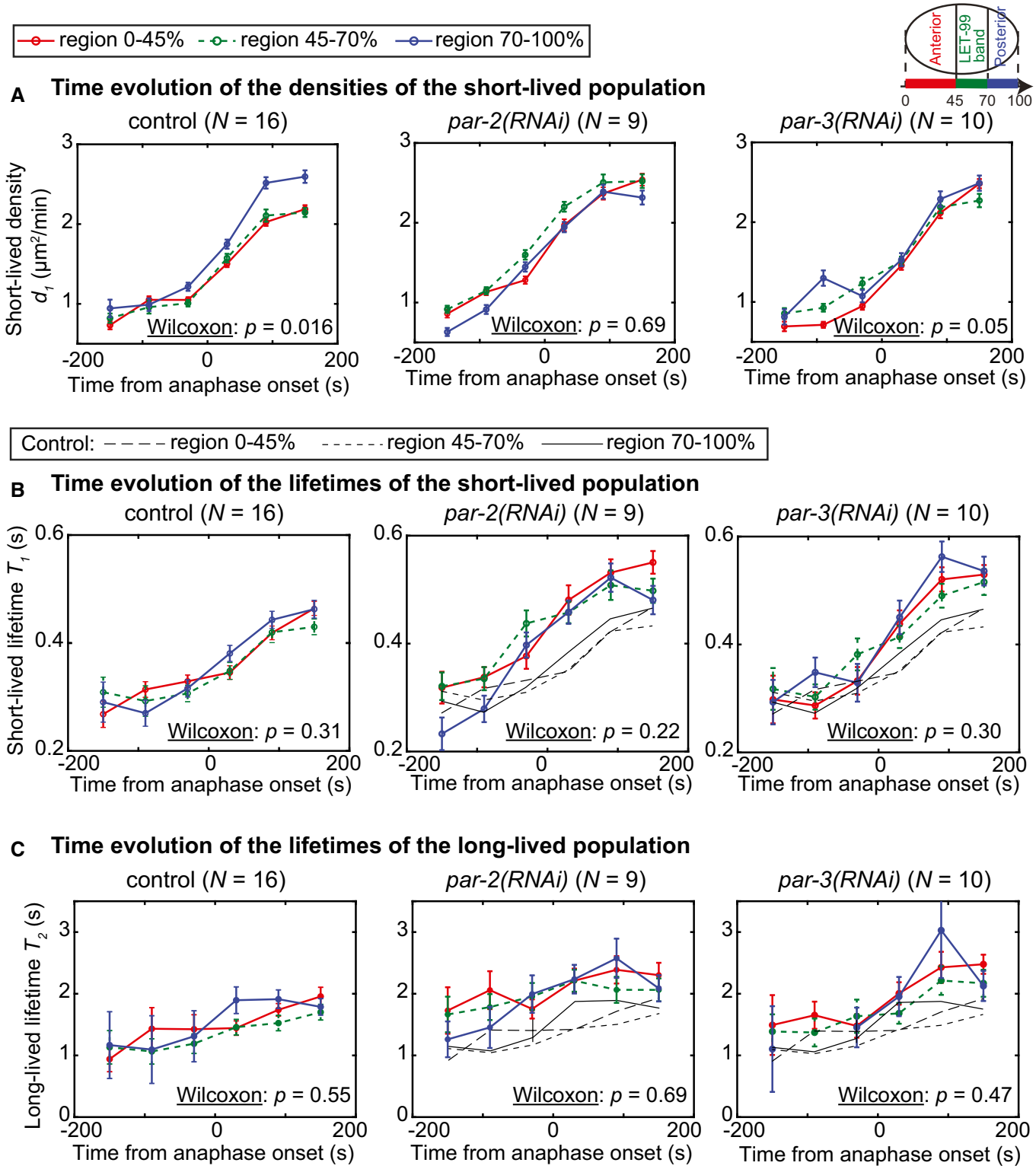

Figure 5.

Figure 5. The PAR proteins control the polarisation of the short-lived microtubule density and the residence time of both populations.

A–C Evolution of the DiLiPop parameters during metaphase and anaphase in (red) the anterior region, (green) the lateral LET-99 band and (blue) the posterior-most region: (A) short-lived densities, (B) short-lived lifetimes, and (C) long-lived lifetimes. The three cortical regions are depicted in the schematics at the top right. We analysed, using 60-s time-blocks, (left) $N = 16$ control embryos, (middle) $N = 9$ *par-2(RNAi)*-treated embryos and (right) $N = 8$ *par-3(RNAi)*-treated embryos. We tested a significant difference between the anterior and posterior-most time-series with the Wilcoxon rank test. In depleted conditions, thin black lines report the corresponding controls.

Data information: Error bars are SD obtained by bootstrapping (Appendix Text, §1.2.5). The data sets composed of *par-2(RNAi)*- or *par-3(RNAi)*-treated embryos are also used in the Appendix Fig S11.
Source data are available online for this figure.

tbg-1(RNAi) treatment and observed a reduced posterior displacement of the spindle (Fig EV4D) (Motegi *et al,* 2006). We measured a lifetime of the long-lived population significantly decreased in anaphase compared to the control one, while the short-lived lifetime was only mildly affected (Fig 6B–D). Consistently, the short-lived and long-lived microtubule lifetime time-series were non-correlated (Pearson $r = 0.45$, χ^2 test $P = 0.36$). It suggested that the short-lived population lifetime was mostly not affected by the centrosome position. Therefore, it implied that a direct or indirect (through the cytoplasm or cortex) regulation of the temporal control by spindle position is unlikely. We measured a decreased density for both populations during anaphase (Fig EV4E) due to the positional control, as expected (Bouvrais *et al,* 2018). These observations suggested that a second mechanism might control the short-lived population, on top of the global regulation previously discussed.

We asked whether the above changes in lifetime evolution could result from an altered regulation of microtubule dynamics or of dynein processivity, due to modified cell cycle progression and particularly of anaphase onset (Srayko *et al,* 2005; McCarthy Campbell *et al,* 2009). To do so, we used the separase activity assay (Kim *et al,* 2015). We performed the same treatments in a strain labelled by mCh::H2B and GFP::sensor, the sensor being a read-out of separase activity (Materials and Methods). We measured fluorescent signal at the chromosomes from nuclear envelope breakdown (NEBD) to mid-anaphase. We observed a decrease in GFP fluorescent signal at about 100 s from NEBD for both the control and *tbg-1 (RNAi)*-treated embryos (Fig 6E). It confirmed that the separase was activated similarly in the two conditions. It suggested a normal temporal control of the dynein processivity and microtubule dynamics upon *tbg-1(RNAi)*. These results agreed with the strong correlation between the short-lived-lifetime time-series of *tbg-1(RNAi)*-treated embryos and their controls (Pearson $r = 0.98$, χ^2 test $P = 7 \times 10^{-4}$). Overall, while a general regulation of the microtubule dynamics exists, we suggested that the short-lived microtubule lifetime increases beyond that regulation. It is consistent with an increasing processivity that causes force build-up (Labbé *et al,* 2004; Pécréaux *et al,* 2006a) and accounts for the mitotic progression control of the cortical pulling force.

To gain certainty about the temporal control of pulling forces through generator processivity, we depleted the ortolog of proteasome 26S subunit ATPase 5 RPT-6^{PSMC5} and delayed the anaphase onset by 30 ± 7 s with respect to NEBD (Appendix Fig S13A) (Campbell *et al,* 2009). It delayed the increase in the short-lived lifetime and the instantaneous contact count correspondingly (Appendix Fig S13C and E). The mild delay in spindle posterior displacement might also contribute to this latter (Appendix Fig S13B). Importantly, setting the reference time to anaphase onset cancelled out the short-lived-lifetime delay further confirming its link with anaphase onset (Appendix Fig S13D). This experiment confirmed that pulling force increase around anaphase onset is associated with longer short-lived lifetime reflecting larger dynein processivity.

Finally, along a complementary line, we prevented chromatid separation by depleting HCP-4^{CENP-C} (Oegema *et al,* 2001; Lewellyn *et al,* 2010) and observed no chromatid separation in $N = 10$ *hcp-4 (RNAi)*-treated embryos (Fig EV5A and B). This was due to a lack of microtubule-kinetochore connection withstanding the tension (Cheeseman *et al,* 2004). We also found a precocious spindle elongation as previously reported (Fig EV5C) (Oegema *et al,* 2001; Lewellyn *et al,* 2010). The time evolution of the short-lived lifetime upon *hcp-4(RNAi)* ($N = 6$) was synchronised with the control ($N = 10$) when using NEBD as reference time (Fig EV5E). Importantly, using the separase assay on *hcp-4(RNAi)*-treated embryos, we observed a decrease in intensity mildly delayed compared to control embryos, revealing that the cell cycle was not delayed upon *hcp-4(RNAi)*, despite no chromatid separation (Fig EV5D). It was in agreement with other studies suggesting that the spindle assembly checkpoint (SAC) is weak during the first division of *C. elegans* embryo (Galli & Morgan, 2016; Gerhold *et al,* 2018). We concluded that the raise of the short-lived lifetime, and thus, pulling force generator processivity is linked to anaphase onset but not to chromatid separation.

Overall, we suggest that the increase in dynein processivity from anaphase onset reflects the mitotic progression. It is linked to the cell cycle but not to chromatid separation and permits the timely spindle posterior displacement.

The polymerising microtubules contribute to maintaining the spindle at the cell centre

We recently proposed, from cell-scale measurements, that the spindle is maintained at the cell centre during metaphase by microtubules pushing against the cortex (Garzon-Coral *et al,* 2016; Pécréaux *et al,* 2016). To test this hypothesis at the microscopic scale, we monitored the long-lived population, which reveals microtubules pushing against the cortex. We varied the long-lived microtubule density by targeting either MAPs (Srayko *et al,* 2005) or polarity proteins (Labbé *et al,* 2003; Severson & Bowerman, 2003). We assessed the quality of centring using the stability of the metaphasic spindle in the cell centre (Pécréaux *et al,* 2016), measured through the diffusion coefficient of the spindle position along the transverse axis D_{Sy} computed from images taken at the spindle plane (Berg-Sørensen & Flyvbjerg, 2004; Nørrelykke & Flyvbjerg, 2010). The smaller this value, the better the centring stability. We found an anti-correlation between this measurement

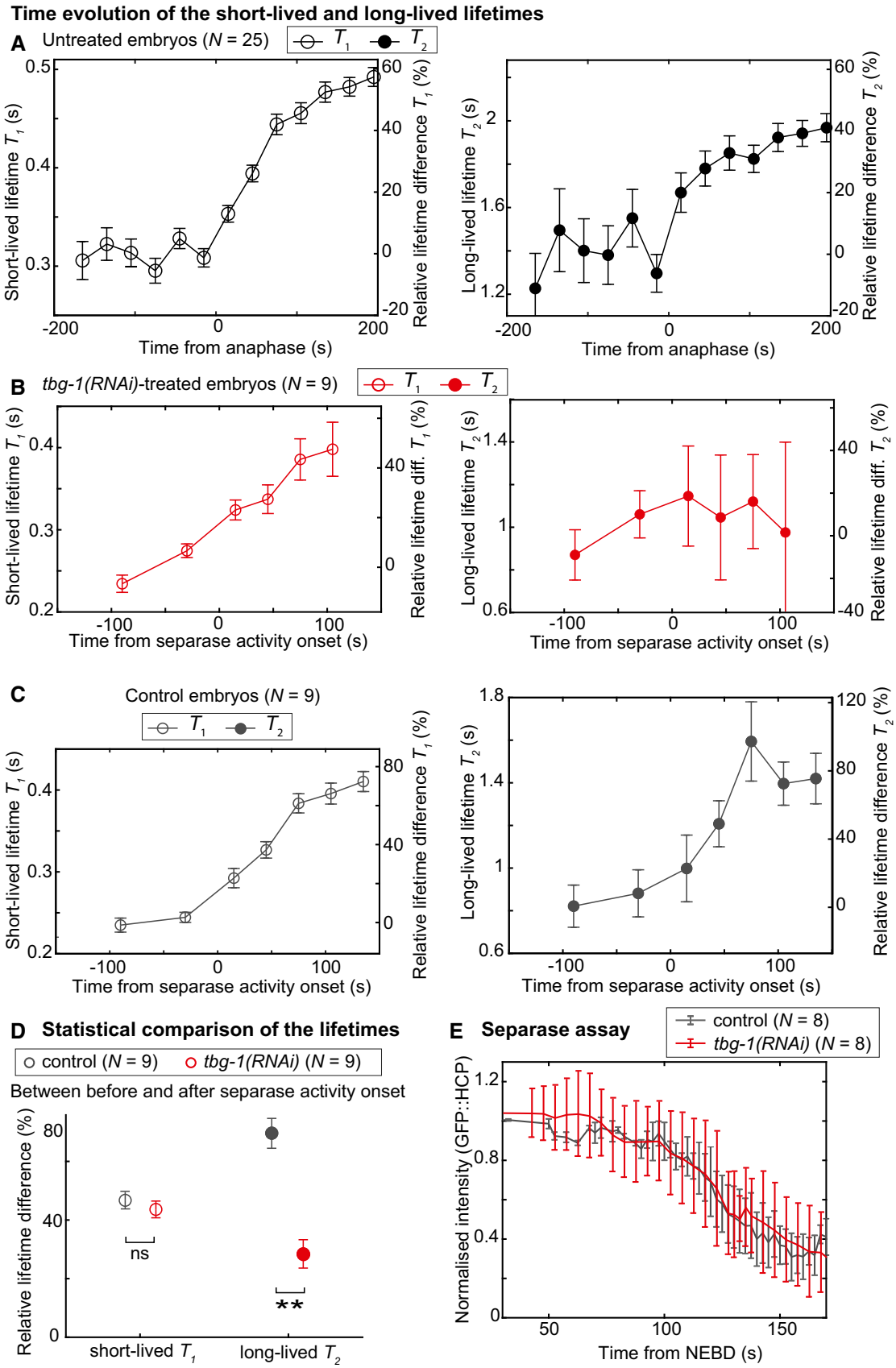

Figure 6.

Figure 6. The short-lived population lifetime increases sharply during mitosis, independently of spindle posterior displacement.

A–C Temporal evolutions of the microtubule lifetimes of (A, black) $N = 25$ untreated embryos for (left) the short-lived and (right) the long-lived populations, (B, red) $N = 9$ *tbg-1(RNAi)*-treated embryos, and (C, grey) their control embryos ($N = 9$). We considered a single region encompassing the whole cortex and used 30-s time-blocks for untreated embryos. For *tbg-1(RNAi)*-treated embryos and their controls, we used 60-s time-blocks during metaphase and 30-s time-blocks during anaphase. Y-scale on the right-hand side displays the lifetime difference relative to the averaged value over metaphase. The long-lived-lifetime time-series of the control and *tbg-1(RNAi)*-treated embryos were independent (Pearson $r = 0.35$, χ^2 test $P = 0.49$), while the short-lived-lifetime ones were correlated ($r = 0.98$, $P = 7 \times 10^{-4}$).

D Differences in short- and long-lived lifetimes between metaphase and early anaphase (from 0 s to 100 s from anaphase onset), normalised by their respective metaphase lifetimes for (red) $N = 9$ *tbg-1(RNAi)*-treated embryos and (grey) $N = 9$ control embryos.

E Mean chromosomal GFP fluorescence of the separase sensor over time, for (red) $N = 8$ *tbg-1(RNAi)*-treated embryos and (grey) $N = 8$ control embryos.

Data information: Error bars are SD obtained (A-D) by bootstrapping (Appendix Text, §1.2.5) or (E) from raw data. In (D), stars indicate significant differences (Student's *t*-test; $^{**}P \leq 0.001$). In (A), the data set composed of $N = 25$ untreated *C. elegans* embryos is also used in the Figs 1E and F, 2A, 4A and B, in Appendix Figs S1A, S4, S6C and D, S12A and B, S14 and Appendix Table S2. The data set composed of *tbg-1(RNAi)*-treated embryos is also used in the Fig EV4.
Source data are available online for this figure.

and the density of long-lived microtubules (Fig 7A) but not with the short-lived density (Fig 7B). These direct observations of force-generating events suggested that microtubules pushing—rather than pulling—contribute to maintaining the spindle at the cell centre. Furthermore, because the microtubule density at the cortex impacted the centring, these results were not consistent with the cytoplasmic pulling hypothesis (Kimura & Kimura, 2011).

Discussion

Through an advanced and careful analysis of microtubule-contact dynamics at the cortex, we monitored the distribution of two microtubule populations distinct by their residence times. Our measured lifetimes, 0.4 and 1.8 s, are similar to previously published values ranging from 1 to 2 s (Kozlowski *et al,* 2007; O'Rourke *et al,* 2010; Lacroix *et al,* 2016; Schmidt *et al,* 2017; Sugioka *et al,* 2018). Not surprisingly, the approaches with higher frame rates, consistent with microtubule growth and shrinkage rates, provided residence times smaller and close to the values found here. In the pioneering work of Labbé *et al* (2003), the measured residence times in the order of 10–15 s resulted from a frame acquisition rate of 0.5 Hz (Labbé *et al,* 2003), likely by linking multiple contacts. Since then, the microtubule dynamics in the nematode appeared exceptionally fast compared to other organisms (Srayko *et al,* 2005; Kozlowski *et al,* 2007; Chaaban *et al,* 2018). Beyond measuring the residence time, we aimed to understand the regulation of the forces positioning the spindle by analysing the statistics of individual events. While the most likely cause of spot disappearing from the cortex is the catastrophe, we cannot exclude that microtubules leave the cortex pulled out faster than their growth rate, as suggested in (Kozlowski *et al,* 2007). Disregarding the cause of spot disappearing, the force generating is stopped. Importantly, we performed our investigations on representative sampling, estimating that DiLiPop recovered about 66% of the microtubule contacts at the cortex, based on electron micrographs (Redemann *et al,* 2017). Overall, our accurate and representative approach enabled us to decipher and quantitatively understand the complex force regulations that conduct the spindle choreography.

The microtubule belonging to a population is a dynamical choice

We claim here that the microtubule dynamics are read-out of the forces positioning the mitotic spindle. Beyond microtubule-associated proteins and molecular motors, we cannot exclude more complex mechanisms creating the three proposed controls. We briefly reviewed here the cytoplasm rheology, the actin-myosin cortex properties and microtubule structural changes. Firstly, several cytoplasmic constituents are asymmetrically segregated during *C. elegans* mitosis (Strome & Wood, 1983; Boyd *et al,* 1996; Hird *et al,* 1996; Guedes & Priess, 1997; Schubert *et al,* 2000). However, no difference of cytoplasmic viscosity has been found comparing the anterior and posterior embryo halves (Daniels *et al,* 2006). Therefore, hydrodynamics are unlikely to play a role in polarity control. Coming to pushing force, it was proposed that bent microtubules, because of buckling, could be reinforced laterally from the cytoplasm (Brangwynne *et al,* 2006; Brangwynne *et al,* 2007; Brangwynne *et al,* 2008; Reymann *et al,* 2016). By altering the pushing force, through the force-velocity relation (Dogterom & Yurke, 1997; Janson & Dogterom, 2004), it could modify the dynamics of the long-lived population and thus the positional control. This is, however, a global effect.

Secondly, we considered the mechanical properties of the cortex itself. Indeed, the cortical actin-myosin network was proposed to generate forces positioning the spindle (Goulding *et al,* 2007). The actin-myosin cortex is reportedly asymmetric during metaphase and anaphase (Munro *et al,* 2004; Motegi & Sugimoto, 2006; Hirani *et al,* 2019). It suggests that the putative role played by the cortex would relate to the polarised pulling forces. In our experiments, the asymmetry of the short-lived population density was identically affected by targeting PAR proteins, also known to control actin-myosin distribution and GPR-1/2, which is independent of NMY-2. It is thus unlikely that the actin-myosin network contributes to regulating the pulling forces. Similarly, cytoplasmic and cortical flows are dependent on polarity proteins (Munro *et al,* 2004) and are unlikely to control the imbalance of pulling force. Using membrane invagination under mild *nmy-2(RNAi)*, preserving polarity, revealed the pulling force generators. By targeting the actin-myosin network regulators, this approach reached the same conclusion (Redemann *et al,* 2010). However, the same authors and others suggested that a mechanically stiff cortex is needed to withstand the pulling force-generating (Kunda *et al,* 2008; Kunda & Baum, 2009). To this respect, actin-myosin can find a global implication, and the cross-talk between microtubule and actin-myosin networks is currently investigated (Preciado Lopez *et al,* 2014b; Colin *et al,* 2018; Dogterom & Koenderink, 2019; Inoue *et al,* 2019).

Correlation between microtubule-densities and spindle-position stability during metaphase

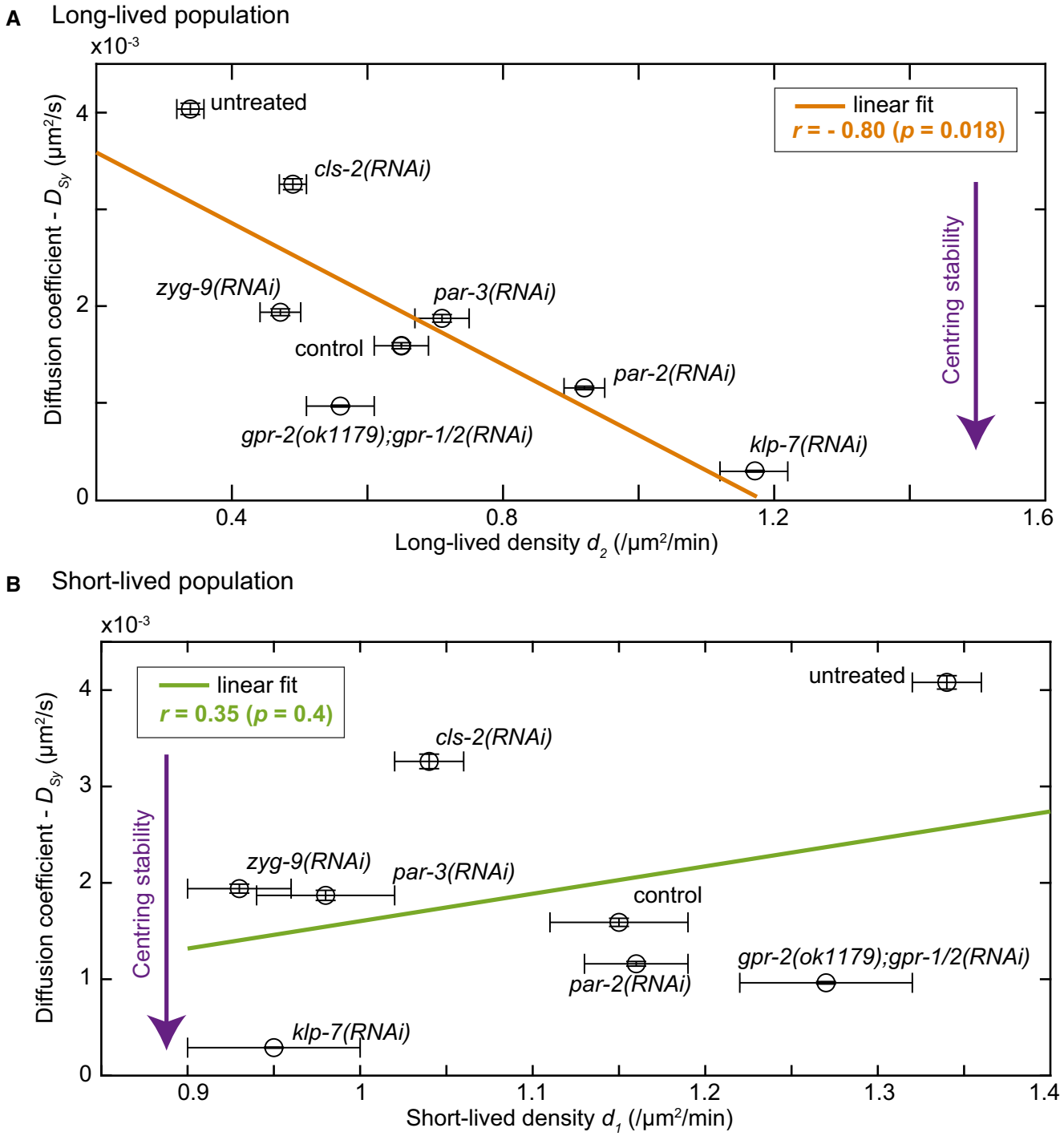

Figure 7. The long-lived microtubules, reflecting pushing forces, contribute to maintaining the spindle at the cell centre.

A, B Diffusion coefficient of the spindle position along the transverse axis, D_{Sy}, characterising the centring stability and based on imaging at the spindle plane, plotted against the density of the (A) long-lived and (B) short-lived microtubule population during metaphase, obtained by DiLiPop analysis of images at the cortex. The orange and green lines depict the Pearson correlations, respectively, for the long-lived ($r = -0.80$, χ^2 test $P = 0.018$) and short-lived populations ($r = 0.35$, $P = 0.4$). We varied the pulling and pushing forces by using *klp-7(RNAi)* ($N = 8$ at the cortex and $N = 9$ at the spindle plane, written as 8/9 for the following conditions), *zyg-9(RNAi)* ($N = 13/8$), *cls-2(RNAi)* ($N = 11/9$), *par-2(RNAi)* ($N = 9/9$), *par-3(RNAi)* ($N = 10/6$), *gpr-2(ok);gpr-1/2(RNAi)* ($N = 8/8$), control embryos ($N = 8/10$) and untreated embryos ($N = 10/10$).

Data information: For short- and long-lived densities, error bars are SD obtained by bootstrapping (Appendix Text, §1.2.5). For the diffusion coefficients, error bars are SE. Source data are available online for this figure.

Next, we wondered whether the post-translational modifications (PTM) could participate in the two-population functions. Indeed, few examples have shown that PTM can directly modulate microtubule dynamics (Chu *et al,* 2011) or can control microtubule dynamics indirectly by regulating MAPs (Peris *et al,* 2009; Lacroix *et al,* 2010). PTM are usually observed for stable microtubules, therefore mostly in neuronal cells in nematode and other species, or in human mitotic cells, e.g. (Wloga & Gaertig, 2010; Janke & Bulinski, 2011; He *et al,* 2020), which contrasts with the high dynamics of *C. elegans* embryo microtubules. Among the possible PTM, tyrosination is the most likely (Peris *et al,* 2006). Indeed, the lack of α-tubulin with a proper site of acetylation in *C. elegans* embryo precludes acetylation (Hurd, 2018). Besides, glutamylation-related enzyme depletion showed only a minor embryonic phenotype and normal microtubule functions (Chawla *et al,* 2016). Consistently, it has been observed that astral microtubules are mostly tyrosinated in human cells (Gundersen & Bulinski, 1986) and *C. elegans* embryo (Barbosa *et al,* 2017). It makes unlikely that tyrosinated versus not could distinguish our two populations. Furthermore, the short lifespan of astral microtubules, less than a minute (Srayko *et al,* 2005; Kozlowski *et al,* 2007), appears hardly compatible with a differential tyrosination, as this is a slower process (Schulze *et al,* 1987; Webster *et al,* 1987a; Webster *et al,* 1987b). Thus, the distinct cortical dynamics of the two populations are unlikely due to differences in PTM state of the microtubules.

Lastly, various tubulin isotypes are present, and we wondered whether different mixes of them could differentiate our microtubule populations. Indeed, tubulin isotype composition can modulate microtubule dynamics (Annapurna *et al,* 2017; Honda *et al,* 2017). However, the labelling of α- or β-tubulin only mildly scaled the lifetimes of the two populations while their proportions were preserved. Such a difference appears too small to support a hypothetical differing isotype composition between our two populations accounting for a distinct lifetime at the cortex.

In a broader take, we interpreted the two populations only as dynamically distinct because of distinct functions, pushing and pulling. Interestingly, upon perturbing by RNAi either microtubule dynamics regulators or the cortical force-generating complex, the population proportions changed but not the total contact count, except if altering the direct regulators of the microtubule network, like KLP-7 or EFA-6. Such an observation suggests that the belonging to a population for a microtubule is a dynamical choice. It depends likely whether the microtubule meets or not a (rare) trimeric force-generating complex at the cortex (Grill & Hyman, 2005; Pécréaux *et al,* 2006a; Park & Rose, 2008; Riche *et al,* 2013; Bouvrais *et al,* 2018). Overall, DiLiPop offers a dynamical read-out of the distribution of force-generating events in space and time.

The short-lived population may also include stalled microtubules

During late anaphase, we measured about 50 short-lived microtubules contacting the visible cortex (Appendix Fig S14), extrapolated to about 150 per half cortex, compared to the reported value, 10–100 per cortex half (Grill *et al,* 2003; Redemann *et al,* 2010). We probably observed some non-pulling events that could correspond to stalled microtubule-ends/dyneins. Indeed, *in vitro* and *in vivo* studies showed that anchored dynein could serve as microtubule plus-end tether (Dujardin & Vallee, 2002; Hendricks Adam *et al,* 2012; Laan *et al,* 2012b; Perlson *et al,* 2013; Yogev *et al,* 2017; Bouvrais *et al,* 2018). It can reveal a mechanism regulating dynein run initiation from a stalled state to bound to a microtubule (Laan *et al,* 2012a; Jha *et al,* 2017).

The pushing force maintains the spindle at the cell centre during metaphase

The final position of the spindle results from the balance of centring and pulling forces (Pécréaux *et al,* 2006a; McNally, 2013; Bouvrais *et al,* 2018). Our approach allowed us to investigate how the spindle is maintained at the cell centre during metaphase at the scale of a single microtubule. Indeed, we recently proposed that the microtubule pushing against the cortex could account for the extraordinary accuracy of this positioning (Pécréaux *et al,* 2016). Consistently, during metaphase, we observed that the density of long-lived microtubules correlates with centring stability. In contrast, the short-lived density measurements appear poorly correlated with centring stability. Furthermore, this latter population displays a reduced density during metaphase compared to anaphase. It is consistent with the pulling force contributing to de-centring (Dogterom *et al,* 2005; Grill & Hyman, 2005; Kozlowski *et al,* 2007; Zhu *et al,* 2010; Garzon-Coral *et al,* 2016; Pécréaux *et al,* 2016).

Recently, the APR-1/APC complex was suggested to decrease the cortical forces anteriorly through reducing the lifetime of force generators at the anterior cortex (Sugioka *et al,* 2018). This study differs by the method used to distinguish populations and our results contrast. We here suggest that the centring force does not contribute to the posterior displacement since we did not observe an increased density or lifetime of the long-lived population anteriorly during anaphase. Our study also supports successive dominance of pushing and pulling along time (Ahringer, 2003; Pécréaux *et al,* 2006a; Garzon-Coral *et al,* 2016; Bouvrais *et al,* 2018) (Appendix Text §3). During metaphase, the pulling force plateaus. It results in only a slow posterior displacement but lets the centring forces dominate by a factor ~2 along the transverse axis. In anaphase, the pulling reinforces in particular because the short-lived-microtubule lifetime undergoes a pronounced increase and the ratio is reversed, favouring pulling. This regulation through intensifying the pulling/displacement forces contrasts with recent findings in the sea urchin zygote, whereby a reduction of the centring forces accounts for the de-centration after the maintenance in cell centre (Sallé *et al,* 2018). In the nematode zygote, pushing force barely superimposes to the pulling one without contributing to the asymmetric positioning of the spindle (Grill & Hyman, 2005; Pécréaux *et al,* 2006a).

With the DiLiPop assay, we can investigate what limits the catastrophe when microtubule grows against the cortex and generates pushing force. One promising candidate as stabilising agent is the CLASP protein (Al-Bassam *et al,* 2010; Elizabeth *et al,* 2018). We indeed measured a specific decrease in the long-lived population upon *cls-2(RNAi)* (Fig EV4). Furthermore, several works have proposed a cross-talk between microtubules and actin recently (Dogterom & Koenderink, 2019). In particular, the actin architecture could regulate differently the microtubules, i.e. unbranched actin filaments preventing microtubule catastrophe (Colin *et al,* 2018). Other indications of such a cross-talk between actin and microtubule are the existence of microtubule actin cross-linking factors (MACF) (Leung *et al,* 1999), the capture of growing microtubules

guided by stiff actin bundles (Preciado Lopez *et al,* 2014a) or the acceleration of actin filament elongation by microtubule plus-end-associated proteins (Henty-Ridilla *et al,* 2016). Thus, actin could also play a role in stabilising the long-lived microtubule at the cortex. The third intracellular network, intermediate filaments (IF), could also be involved. They were proposed to stabilise microtubule and also link to actin during mitosis (Duarte *et al,* 2019). Furthermore, IF accumulation can stabilise microtubules in *C. elegans* motor neurons (Kurup *et al,* 2018). In future work, such a cross-talk could also be challenged with our DiLiPop assay in association with the labelling of the actin-myosin network.

The cortical pulling control is threefold, by mitotic progression, polarity and the spindle position

We recently proposed that a second regulation of the pulling force, by the position of the centrosomes, superimposed to the mitotic progression control reflected in the processivity of the force generators (Fig 8, respectively, left and right blocks) (Pécréaux *et al,* 2006a; Bouvrais *et al,* 2018). The DiLiPop sheds light on the interplay of these controls with the polarity one reflected in the asymmetry of dynein on-rate (Fig 8, middle block) (Rodriguez-Garcia *et al,* 2018). Beyond confirming that the dynein detachment rate does not encode the polarity (Fig 8, mixed pink/purple boxes) (Rodriguez-Garcia *et al,* 2018), we found no other cause of force imbalance. Importantly, we observed that this asymmetry is set early in the division and is scaled up by the global and symmetric increase in processivity viewed through short-lived microtubule lifetime (Fig 8, purple boxes). Such a mitotic progression control is consistent with the previous measurements at the cell scale (Labbé *et al,* 2004; Pécréaux *et al,* 2006a; McCarthy Campbell *et al,* 2009). This scaling is likely not gradual. Indeed, we observed a steep increase in the cortical residence time at anaphase onset.

Finally, the DiLiPop suggests that the positional control only reinforces the anteroposterior imbalance of cortical pulling forces in late anaphase (Fig 8, grey box). Consistently, the long-lived microtubule density becomes slightly asymmetric only in late anaphase (Riche *et al,* 2013; Bouvrais *et al,* 2018). While not polarised in early mitosis, this control is affected by PAR-2/PAR-3 proteins, which decrease microtubule lifetimes of both populations (Fig 8, green box). The positional control contributes to force imbalance in late anaphase, and this mechanism depends on the posterior-most

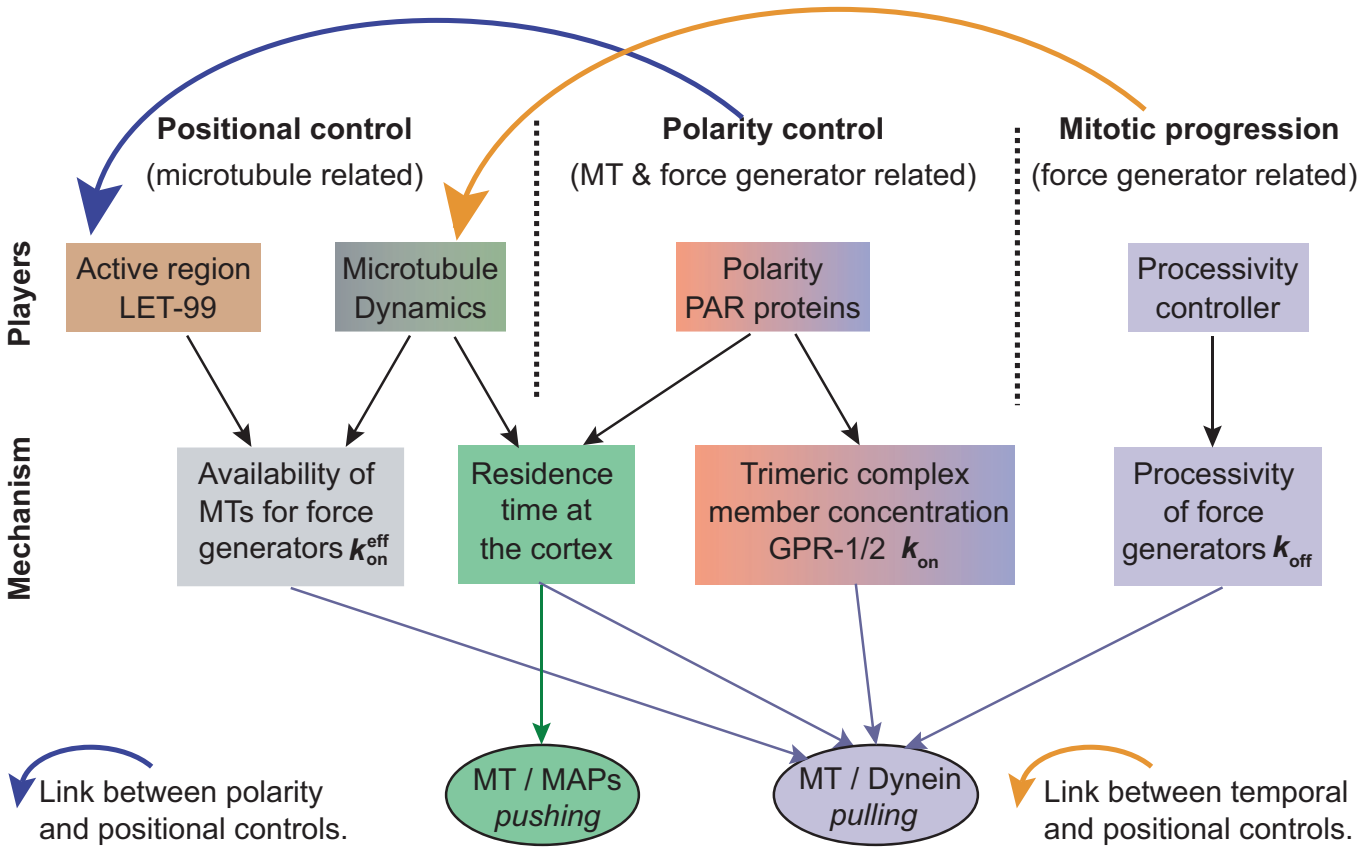

Figure 8. The cortical pulling control is threefold, by mitotic progression, polarity and spindle position.

Schematics of the regulation of the forces that position the spindle with the players (top row) and the quantity regulated (middle row). Grey and brown colours correspond to the positional control involving astral microtubule (MT) dynamics and the active region created by LET-99 band. Purple colour depicts the time control through force generator processivity. Pink/purple colours correspond to the polarity control involving the distribution of the force generators. The latter control also participates in setting the microtubule residence time at the cortex (green).

region created by the LET-99 protein (Fig 8, brown box). Establishing this protein domain is under the control of the polarity (Fig 8, top blue arrow) (Wu & Rose, 2007; Krueger *et al,* 2010; Wu *et al,* 2017). This cross-talk creates a link between the polarity and the positional controls. On the side of the mitotic progression, the cell cycle controls the number of nucleated microtubules, known to increase at anaphase onset (Srayko *et al,* 2005). It increases the microtubule density of both populations, symmetrically, connecting mitotic and positional controls (Fig 8, top orange arrow). However, such a link is loose, and the controls remain mostly independent (Bouvrais *et al,* 2018).

Overall, we propose that the pulling forces are under three independent controls: polarity acting through the force generator on-rate due to an asymmetric distribution of GPR-1/2; mitotic progression, corresponding to the processivity of the force generators; positional control, due to the availability of the microtubules at the cortex. The centring mechanism is due to microtubules pushing against the cortex and merely superimposes to the pulling forces. Beyond these findings, this work exemplifies the interest of combining investigations at two scales. In particular, it offers the unparalleled ability to view the individual pulling and pushing force-generating events. We foresee that this novel approach will find applications beyond cell division.

Materials and Methods

Culturing *C. elegans*

Caenorhabditis elegans nematodes were cultured as described in (Brenner, 1974) and dissected to obtain embryos. The strains were maintained at 25°C and imaged at 23°C. The strains were handled on nematode medium plates and fed with OP50 bacteria.

Strains of *C. elegans* and *C. briggsae* used

Caenorhabditis elegans TH65 YFP::TBA-2 (α-tubulin) strain (Srayko *et al,* 2005) having a fluorescent labelling of the whole microtubule (MT) was used for the DiLiPop assay as well as *C. elegans* AZ244 GFP::TBB-2 (β-tubulin) strain (Praitis *et al,* 2001), *C. elegans* JEP68 YFP::TBA-2 (α-tubulin); HIS-58::mCherry strain and *C. briggsae* ANA020 GFP::TBB (β-tubulin) strain. TH65 and JEP68 strains were also the standard for the "centrosome-tracking" assay used to validate the penetrance of RNAi treatments. TH66 EBP-2::GFP strain (Srayko *et al,* 2005) that displays a labelling of microtubule plus-ends was used for comparison of its effects on microtubule dynamics. The JEP18 *gpr-2(ok1179)* strain was used to target GPR-1/2 protein though a mutation. The OD2207 strain, expressing HIS-58 fused to mCherry and a sensor composed of the CPAR-1N-tail fused to the histone fold domain (HFD) of HCP-3 and GFP, was used for the separase assay (Kim *et al,* 2015).

Gene inactivation through protein depletion by RNAi feeding

RNA interference (RNAi) experiments were performed by feeding using the Ahringer-Source BioScience library (*cls-2* : III-4J10; *csnk-1* : I-5K03; *efa-6* : IV-6P21; *gpr-1/-2* : III-4J09; *hcp-4* : I-1L17; *klp-7* : III-5B24; *lin-5* : II-5J10; *par-2* : III-1K08; *par-3* : III-3A01; *rpt-6* : III-6C12; *tbg-1* : III-5K19; *zyg-9* : II-6M11) (Kamath & Ahringer, 2003), except for GOA-1;GPA-16 depletion, whose clone was kindly given by Prof P. Gönczy. The feedings were performed at 25°C for various durations according to the experimental goals. The treatment lasted 24h for *rpt-6*, *tbg-1*, *lin-5*, *goa-1*;*gpa-16* and *klp-7* genes. When we aimed for stronger phenotypes (e.g. symmetric divisions), we used duration of 48h (*hcp-4*, *cls-2*, *par-2*, *par-3* and *gpr-1/2*). The duration was reduced to 4h, 6-10h and 16h when targeting *zyg-9*, *efa-6* and *cnsk-1*, respectively. The control embryos for the RNAi experiments were fed with bacteria carrying the empty plasmid L4440. We did not notice any phenotype suggesting that the meiosis was impaired during these various treatments.

Preparation of the embryos for imaging

Embryos were dissected in M9 buffer and mounted on a pad (2% w/v agarose, 0.6% w/v NaCl, 4% w/v sucrose) between a slide and a coverslip. Depending on the assay (landing or centrosome-tracking ones), embryos were observed using different microscopic setups. To confirm the absence of phototoxicity and photodamage, we checked for normal rates of subsequent divisions (Riddle *et al,* 1997; Tinevez, 2012). Fluorescent lines were imaged at 23°C.

Imaging of microtubule contacts at the cortex

We imaged *C. elegans* one-cell embryos at the cortex plane in contact with the glass slide, viewing from the nuclear envelope breakdown (NEBD) until late anaphase. We used a Leica DMi8 spinning disc microscope with Adaptive Focus Control (AFC) and a HCX Plan Apo 100×/1.4 NA oil objective. Illumination was performed using a laser with emission wavelength of 488 nm, and we used GFP/FITC 4 nm band pass excitation filter and a Quad Dichroic emission filter. To account for the fast microtubule dynamics at the cortex, images were acquired at an exposure time of 100 ms (10 Hz), except otherwise stated, using an ultra-sensitive Roper Evolve EMCCD camera. The setup was controlled by the Inscoper device. During the experiments, the embryos were kept at 23°C. To image embryos at the cortex, we typically moved the focus to 12–15 μm below the spindle plane. Images were then stored using OMERO software (Li *et al,* 2016).

Spindle pole imaging

Embryos were observed at the midplane using a Zeiss Axio Imager upright microscope modified for long-term time-lapse. First, an extra anti-heat filter was added to the mercury lamp light path. Secondly, to decrease the bleaching and obtain optimal excitation, we used an enhanced transmission 12 nm band pass excitation filter centred on 485 nm (AHF analysentechnik). We used a 100×/1.45 NA Oil plan Apo objective. Images were acquired with an Andor iXon3 EMCCD 512 × 512 camera at 33 frames per second and using the Solis software. Images were then stored using OMERO software (Li *et al,* 2016).

Centrosome-tracking assay

The tracking of labelled centrosomes and analysis of trajectories were performed by a custom tracking software (Pécréaux *et al,* 2006a; Pécréaux *et al,* 2016) and developed using Matlab (The MathWorks). Tracking of −20°C methanol-fixed γ-tubulin-labelled

embryos indicated accuracy to 10 nm. Embryo orientations and centres were obtained by cross-correlation of embryo background cytoplasmic fluorescence with artificial binary images mimicking embryos, or by contour detection of the cytoplasmic membrane using background fluorescence of cytoplasmic YFP::TBA-2 with the help of an active contour algorithm (Pécréaux *et al,* 2006b). The results were averaged over all of the replicas for each condition.

Simulation of microscopy images

To validate the image-processing pipeline (Appendix Fig S5), we built fluorescence images of known dynamics, which mimic our cortical images using the algorithm developed by (Costantino *et al,* 2005) that we adapted to our needs as previously done (Bouvrais *et al,* 2018). In further details, we simulated stochastic trajectories of particles that displayed a limited random motion characterised by the diffusion coefficient D. We sampled the duration of the tracks from an exponential distribution. We encoded the fluorescence intensity through the quantum yield parameter (Qyield). After plotting the instantaneous positions, we mimicked (i) the effect of the point-spread function (PSF) in fluorescence microscopy by applying a Gaussian filter and (ii) the background noise by adding at each pixel a sampling of a Gaussian distribution. Details of the parameters used for simulation can be found in Appendix Table S3.

Separase sensor assay

To check whether the cell cycle was unaffected by the *tbg-1(RNAi)* or *hcp-4(RNAi)* treatment, we performed the separase sensor assay introduced in (Kim *et al,* 2015) using the strain OD2207 (Figs 6E and EV5D). We acquired 5×2 μm z-stacks every 2.5 s from NEBD to post-chromatids-separation. To quantify fluorescence, we used ImageJ (Fiji) and followed the image-processing protocol described in (Kim *et al,* 2015).

Nocodazole treatment

L4 worms were grown on *perm-1(RNAi)* feeding plates at 25°C for 20 h and then dissected in an open imaging chamber filled with egg buffer (118 mM NaCl, 48 mM KCl, 2 mM $CaCl_2$, 2 mM $MgCl_2$, 25 mM HEPES, pH 7.3) (Zhang *et al,* 2011). A nocodazole solution was added around NEBD to reach a final concentration of 10 μg/ml. It led to the loss of tubulin fluorescent signal from the centrosomes, astral and spindle microtubules after less than a minute, similarly to (Carvalho *et al,* 2011) (Appendix Fig S2A).

Characterisation of microtubule track motion at the cortex

To compute the displacement of the microtubules contacting the cortex, for each track, we summed the displacements of the microtubule contacts between frames, using the x and y coordinates of each contact. We averaged the total displacement among all microtubule tracks and then among the embryos of a given condition. We also classified the tracks as linear (directive) or random (diffusive) according to their asymmetry, as done in (Huet *et al,* 2006; Jaqaman *et al,* 2008). This classification is based on the asymmetry in the scatter of microtubule-contact positions along each track. Tracks shorter than 3 frames were ignored. We chose an alpha parameter (the classification threshold) of 0.1 (90^{th} percentile).

Statistics

For classic statistical analyses, averaged values of two conditions were compared using the two-tailed Student's t-test with correction for unequal variance except where otherwise stated. The Wilcoxon signed-rank test was used to assess whether two time-series of DiLiPop densities/lifetimes were significantly different all along. The Pearson χ^2 test was used to indicate whether two sets of data were correlated or independent. For the sake of simplicity, we recorded confidence levels using diamond or stars (◦, $P \leq 0.05$; *, $P \leq 0.01$; **, $P \leq 0.001$; ***, $P \leq 0.0001$; ****, $P \leq 0.00001$) and ns (non-significant, $P > 0.05$; sometimes omitted to save room). We abbreviated standard deviation by SD, standard error by SE, and standard error of the mean by SEM.

Data and image processing

All data analysis was developed using Matlab (The MathWorks).

Data availability

The code of the DiLiPop analysis from this publication has been deposited to Zenodo database (https://www.zenodo.org) and assigned the identifier: https://doi.org/10.5281/zenodo.4552485.

Expanded View for this article is available online.

Acknowledgements
The bacterial clone of GPA-16;GOA-1 was a kind gift from Prof P. Gönczy. We thank Dr. Gregoire Michaux for the feeding clone library and technical support. We also thank Drs. Giulia Bertolin, Aurélien Bidaud-Meynard, Christophe Heligon, Sébastien Huet, Benjamin Mercat, Grégoire Michaux, Anne Pacquelet, Xavier Pinson and Marc Tramier for discussions about the project. Some strains were provided by the Caenorhabditis Genetics Center (CGC), which is funded by National Institutes of Health Office of Research Infrastructure Programs (P40 OD010440; University of Minnesota). JP was supported by a Centre National de la Recherche Scientifique (CNRS) ATIP starting grant and La Ligue nationale contre le cancer. We also acknowledge Plan Cancer (grant BIO2013-02), COST EU action BM1408 (GENiE), RTR siscom (CK as co-ordinator) and La Ligue contre le cancer (comités d'Ille-et-Vilaine et du Maine-et-Loire). Microscopy imaging was performed at the Microscopy Rennes Imaging Center, UMS 3480 CNRS/US 18 INSERM/University of Rennes 1. Spinning disc microscope was co-funded by the CNRS, Rennes Métropole (AIS 16C0400) and Région Bretagne (AniDyn-MTgrant). DF's postdoctoral fellowship was funded by Région Bretagne (pRISM grant). HB's postdoctoral fellowship was funded by the European Molecular Biology Organization (ALTF 326-2013). TP was supported by the France-BioImaging infrastructure (ANR-10-INBS-04).

Author contributions
Conceptualisation: HB, JP; Data curation: HB, LC; Formal analysis: HB, YLC, JP; Funding acquisition: HB, JP; Investigation: HB, LC, DF, NS, SP; Methodology: HB, LC, JP; Project administration: HB, JP; Resources: TP, CK; Software: HB, YLC, TP, CK, JP; Supervision: HB, JP; Validation: HB, LC, DF, NS; Visualisation: HB, JP; Writing – original draft: HB, JP; Writing – review and editing: HB, LC, YLC, DF, JP.

Conflict of interest

The authors declare that they have no conflict of interest.

References

Afshar K, Willard FS, Colombo K, Johnston CA, McCudden CR, Siderovski DP, Gönczy P (2004) RIC-8 is required for GPR-1/2-dependent gα function during asymmetric division of *C. elegans* embryos. *Cell* 119: 219 – 230

Afshar K, Willard FS, Colombo K, Siderovski DP, Gönczy P (2005) Cortical localization of the Gα protein GPA-16 requires RIC-8 function during *C. elegans* asymmetric cell division. *Development* 132: 4449 – 4459

Agresti A (2013) *Categorical data analysis*, Hoboken, NJ: Wiley

Ahringer J (2003) Control of cell polarity and mitotic spindle positioning in animal cells. *Curr Opin Cell Biol* 15: 73 – 81

Al-Bassam J, Kim H, Brouhard G, van Oijen A, Harrison SC, Chang F (2010) CLASP promotes microtubule rescue by recruiting tubulin dimers to the microtubule. *Dev Cell* 19: 245 – 258

Annapurna V, Joseph A, Jeffrey OS, Carolyn AM, Antonina R-M, Laurent B (2017) Tubulin isoform composition tunes microtubule dynamics. *Mol Biol Cell* 28: 3564 – 3572

Barbosa DJ, Duro J, Prevo B, Cheerambathur DK, Carvalho AX, Gassmann R (2017) Dynactin binding to tyrosinated microtubules promotes centrosome centration in *C. elegans* by enhancing dynein-mediated organelle transport. *PLoS Genet* 13: e1006941

Basset A, Boulanger J, Salamero J, Bouthemy P, Kervrann C (2015) Adaptive spot detection with optimal scale selection in fluorescence microscopy images. *IEEE Trans Image Process* 24: 4512 – 4527

Beechem JM (1992) Global analysis of biochemical and biophysical data. *Numerical Computer Methods* 210: 37 – 54

Bellanger J-M, Gönczy P (2003) TAC-1 and ZYG-9 form a complex that promotes microtubule assembly in *C. elegans* embryos. *Curr Biol* 13: 1488 – 1498

Berg-Sørensen K, Flyvbjerg H (2004) Power spectrum analysis for optical tweezers. *Rev Sci Instrum* 75: 594 – 612

Bicout DJ (1997) Green's functions and first passage time distributions for dynamic instability of microtubules. *Phys Rev E* 56: 6656 – 6667

Bieling P, Laan L, Schek H, Munteanu EL, Sandblad L, Dogterom M, Brunner D, Surrey T (2007) Reconstitution of a microtubule plus-end tracking system in vitro. *Nature* 450: 1100 – 1105

Bolker BM (2008) *Ecological models and data in R*. Princeton, NJ: Princeton University Press

Boulanger J, Kervrann C, Bouthemy P, Elbau P, Sibarita JB, Salamero J (2010) Patch-based nonlocal functional for denoising fluorescence microscopy image sequences. *IEEE Trans Med Imaging* 29: 442 – 454

Bouvrais H, Chesneau L, Pastezeur S, Fairbrass D, Delattre M, Pécréaux J (2018) Microtubule feedback and LET-99-dependent control of pulling forces ensure robust spindle position. *Biophys J* 115: 2189 – 2205

Boyd L, Guo S, Levitan D, Stinchcomb DT, Kemphues KJ (1996) PAR-2 is asymmetrically distributed and promotes association of P granules and PAR-1 with the cortex in *C. elegans* embryos. *Development* 122: 3075 – 3084

Brangwynne CP, Koenderink GH, MacKintosh FC, Weitz DA (2008) Nonequilibrium microtubule fluctuations in a model cytoskeleton. *Phys Rev Lett* 100: 118104

Brangwynne CP, MacKintosh FC, Kumar S, Geisse NA, Talbot J, Mahadevan L, Parker KK, Ingber DE, Weitz DA (2006) Microtubules can bear enhanced compressive loads in living cells because of lateral reinforcement. *J Cell Biol* 173: 733 – 741

Brangwynne CP, MacKintosh F, Weitz DA (2007) Force fluctuations and polymerization dynamics of intracellular microtubules. *Proc Natl Acad Sci USA* 104: 16128 – 16133

Brenner S (1974) The genetics of *Caenorhabditis elegans*. *Genetics* 77: 71 – 94

Brouhard GJ, Stear JH, Noetzel TL, Al-Bassam J, Kinoshita K, Harrison SC, Howard J, Hyman AA (2008) XMAP215 is a processive microtubule polymerase. *Cell* 132: 79 – 88

Campbell EKM, Werts AD, Goldstein B (2009) A cell cycle timer for asymmetric spindle positioning. *PLoS Biol* 7: e1000088

Carvalho A, Olson SK, Gutierrez E, Zhang K, Noble LB, Zanin E, Desai A, Groisman A, Oegema K (2011) Acute drug treatment in the early *C. elegans* embryo. *PLoS One* 6: e24656

Chaaban S, Jariwala S, Hsu CT, Redemann S, Kollman JM, Muller-Reichert T, Sept D, Bui KH, Brouhard GJ (2018) The structure and dynamics of *C. elegans* tubulin reveals the mechanistic basis of microtubule growth. *Dev Cell* 47: 191 – 204

Chawla DG, Shah RV, Barth ZK, Lee JD, Badecker KE, Naik A, Brewster MM, Salmon TP, Peel N (2016) *Caenorhabditis elegans* glutamylating enzymes function redundantly in male mating. *Biol Open* 5: 1290 – 1298

Cheeseman IM, MacLeod I, Yates JR, Oegema K, Desai A (2005) The CENP-F-like proteins HCP-1 and HCP-2 target CLASP to kinetochores to mediate chromosome segregation. *Curr Biol* 15: 771 – 777

Cheeseman IM, Niessen S, Anderson S, Hyndman F, Yates JR, Oegema K, Desai A (2004) A conserved protein network controls assembly of the outer kinetochore and its ability to sustain tension. *Genes Dev* 18: 2255 – 2268

Chenouard N, Bloch I, Olivo-Marin JC (2013) Multiple hypothesis tracking for cluttered biological image sequences. *IEEE Trans Pattern Anal Mach Intell* 35: 2736 – 3750

Chenouard N, Smal I, De Chaumont F, Maška M, Sbalzarini IF, Gong Y, Cardinale J, Carthel C, Coraluppi S, Winter M (2014) Objective comparison of particle tracking methods. *Nat Methods* 11: 281 – 289

Chu C-W, Hou F, Zhang J, Phu L, Loktev AV, Kirkpatrick DS, Jackson PK, Zhao Y, Zou H (2011) A novel acetylation of β-tubulin by San modulates microtubule polymerization via down-regulating tubulin incorporation. *Mol Biol Cell* 22: 448 – 456

Colin A, Singaravelu P, Théry M, Blanchoin L, Gueroui Z (2018) Actin-network architecture regulates microtubule dynamics. *Curr Biol* 28: 2647 – 2656.e2644

Colombo K, Grill SW, Kimple RJ, Willard FS, Siderovski DP, Gonczy P (2003) Translation of polarity cues into asymmetric spindle positioning in *Caenorhabditis elegans* embryos. *Science* 300: 1957

Costantino S, Comeau JW, Kolin DL, Wiseman PW (2005) Accuracy and dynamic range of spatial image correlation and cross-correlation spectroscopy. *Biophys J* 89: 1251 – 1260

Couwenbergs C, Labbé J-C, Goulding M, Marty T, Bowerman B, Gotta M (2007) Heterotrimeric G protein signaling functions with dynein to promote spindle positioning in *C. elegans*. *J Cell Biol* 179: 15 – 22

Daniels BR, Masi BC, Wirtz D (2006) Probing single-cell micromechanics in vivo: the microrheology of *C. elegans* developing embryos. *Biophys J* 90: 4712 – 4719

Dogterom M, Kerssemakers JWJ, Romet-Lemonne G, Janson ME (2005) Force generation by dynamic microtubules. *Curr Opin Cell Biol* 17: 67 – 74

Dogterom M, Koenderink GH (2019) Actin-microtubule crosstalk in cell biology. *Nat Rev Mol Cell Biol* 20: 38 – 54

Dogterom M, Yurke B (1997) Measurement of the force-velocity relation for growing microtubules. *Science* 278: 856 – 860

Duarte S, Viedma-Poyatos Á, Navarro-Carrasco E, Martínez AE, Pajares MA, Pérez-Sala D (2019) Vimentin filaments interact with the actin cortex in mitosis allowing normal cell division. *Nat Commun* 10: 4200

Duellberg C, Cade NI, Holmes D, Surrey T (2016) The size of the EB cap determines instantaneous microtubule stability. *Elife* 5: e13470

Dujardin DL, Vallee RB (2002) Dynein at the cortex. *Curr Opin Cell Biol* 14: 44 – 49

Efron B, Tibshirani RJ (1993) *An introduction to the bootstrap*. London: Chapman & Hall

Elizabeth JL, Göker A, Stephen RN, Marija Z (2018) Human CLASP2 specifically regulates microtubule catastrophe and rescue. *Mol Biol Cell* 29: 1168 – 1177

Espiritu EB, Krueger LE, Ye A, Rose LS (2012) CLASPs function redundantly to regulate astral microtubules in the *C. elegans* embryo. *Dev Biol* 368: 242 – 254

Faivre-Moskalenko C, Dogterom M (2002) Dynamics of microtubule asters in microfabricated chambers: the role of catastrophes. *Proc Natl Acad Sci USA* 99: 16788 – 16793

Fielmich L-E, Schmidt R, Dickinson DJ, Goldstein B, Akhmanova A, Van den Heuvel S (2018) Optogenetic dissection of mitotic spindle positioning in vivo. *Elife* 7: e38198

Floyd DL, Harrison SC, van Oijen AM (2010) Analysis of kinetic intermediates in single-particle dwell-time distributions. *Biophys J* 99: 360 – 366

Galli M, Morgan DO (2016) Cell size determines the strength of the spindle assembly checkpoint during embryonic development. *Dev Cell* 36: 344 – 352

Garzon-Coral C, Fantana HA, Howard J (2016) A force-generating machinery maintains the spindle at the cell center during mitosis. *Science* 352: 1124 – 1127

Gerhold AR, Poupart V, Labbé J-C, Maddox PS (2018) Spindle assembly checkpoint strength is linked to cell fate in the *Caenorhabditis elegans* embryo. *Mol Biol Cell* 29: 1435 – 1448

Gigant E, Stefanutti M, Laband K, Gluszek-Kustusz A, Edwards F, Lacroix B, Maton G, Canman JC, Welburn JPI, Dumont J (2017) Inhibition of ectopic microtubule assembly by the kinesin-13 KLP-7 prevents chromosome segregation and cytokinesis defects in oocytes. *Development* 144: 1674 – 1686

Gönczy P (2008) Mechanisms of asymmetric cell division: flies and worms pave the way. *Nat Rev Mol Cell Biol* 9: 355 – 366

Gonczy P, Pichler S, Kirkham M, Hyman AA (1999) Cytoplasmic dynein is required for distinct aspects of MTOC positioning, including centrosome separation, in the one cell stage *Caenorhabditis elegans* embryo. *J Cell Biol* 147: 135 – 150

Gotta M, Ahringer J (2001) Distinct roles for Galpha and Gbetagamma in regulating spindle position and orientation in *Caenorhabditis elegans* embryos. *Nat Cell Biol* 3: 297 – 300

Gotta M, Dong Y, Peterson YK, Lanier SM, Ahringer J (2003) Asymmetrically distributed *C. elegans* homologs of AGS3/PINS control spindle position in the early embryo. *Curr Biol* 13: 1029 – 1037

Goulding MB, Canman JC, Senning EN, Marcus AH, Bowerman B (2007) Control of nuclear centration in the *C. elegans* zygote by receptor-independent Gα signaling and myosin II. *J Cell Biol* 178: 1177 – 1191

Grill SW, Gönczy P, Stelzer EHK, Hyman AA (2001) Polarity controls forces governing asymmetric spindle positioning in the *Caenorhabditis elegans* embryo. *Nature* 409: 630 – 633

Grill SW, Howard J, Schaffer E, Stelzer EHK, Hyman AA (2003) The distribution of active force generators controls mitotic spindle position. *Science* 301: 518

Grill SW, Hyman AA (2005) Spindle positioning by cortical pulling forces. *Dev Cell* 8: 461 – 465

Grinvald A, Steinberg IZ (1974) On the analysis of fluorescence decay kinetics by the method of least-squares. *Anal Biochem* 59: 583 – 598

Grishchuk EL, Molodtsov MI, Ataullakhanov FI, McIntosh JR (2005) Force production by disassembling microtubules. *Nature* 438: 384

Guedes S, Priess JR (1997) The *C. elegans* MEX-1 protein is present in germline blastomeres and is a P granule component. *Development* 124: 731 – 739

Gundersen GG, Bulinski JC (1986) Distribution of tyrosinated and nontyrosinated alpha-tubulin during mitosis. *J Cell Biol* 102: 1118 – 1126

Gusnowski EM, Srayko M (2011) Visualization of dynein-dependent microtubule gliding at the cell cortex: implications for spindle positioning. *J Cell Biol* 194: 377 – 386

He K, Ling K, Hu J (2020) The emerging role of tubulin posttranslational modifications in cilia and ciliopathies. *Biophys Rep* 6: 89 – 104

Hendricks Adam G, Lazarus Jacob E, Perlson E, Gardner Melissa K, Odde David J, Goldman Yale E, Holzbaur Erika LF (2012) Dynein tethers and stabilizes dynamic microtubule plus ends. *Curr Biol* 22: 632 – 637

Henty-Ridilla JL, Rankova A, Eskin JA, Kenny K, Goode BL (2016) Accelerated actin filament polymerization from microtubule plus ends. *Science* 352: 1004 – 1009

Hirani N, Illukkumbura R, Bland T, Mathonnet G, Suhner D, Reymann A-C, Goehring NW (2019) Anterior-enriched filopodia create the appearance of asymmetric membrane microdomains in polarizing *C. elegans* zygotes. *J Cell Sci* 132: jcs230714

Hird SN, Paulsen JE, Strome S (1996) Segregation of germ granules in living *Caenorhabditis elegans* embryos: cell-type-specific mechanisms for cytoplasmic localisation. *Development* 122: 1303 – 1312

Honda Y, Tsuchiya K, Sumiyoshi E, Haruta N, Sugimoto A (2017) Tubulin isotype substitution revealed that isotype combination modulates microtubule dynamics in *C. elegans* embryos. *J Cell Sci* 130: 1652 – 1661

Howard J (2006) Elastic and damping forces generated by confined arrays of dynamic microtubules. *Phys Biol* 3: 54

Howard J, Garzon-Coral C (2017) Physical limits on the precision of mitotic spindle positioning by microtubule pushing forces. *BioEssays* 39: 1700122

Huet S, Karatekin E, Tran VS, Fanget I, Cribier S, Henry J-P (2006) Analysis of transient behavior in complex trajectories: application to secretory vesicle dynamics. *Biophys J* 91: 3542 – 3559

Hurd DD (2018) Tubulins in *C. elegans*. *WormBook* https://doi.org/10.1895/wormbook.1.182.1

Hyenne V, Tremblay-Boudreault T, Velmurugan R, Grant BD, Loerke D, Labbé J-C (2012) RAB-5 controls the cortical organization and dynamics of PAR proteins to maintain *C. elegans* early embryonic polarity. *PLoS One* 7: e35286

Inoue D, Obino D, Pineau J, Farina F, Gaillard J, Guerin C, Blanchoin L, Lennon-Duménil AM, Théry M (2019) Actin filaments regulate microtubule growth at the centrosome. *EMBO J* 38: e99630

Jae Myung I, Forster M, Browne MW (2000) Special issue on model selection

James DR, Ware WR (1985) A fallacy in the interpretation of fluorescence decay parameters. *Chem Phys Lett* 120: 455 – 459

Janke C, Bulinski JC (2011) Post-translational regulation of the microtubule cytoskeleton: mechanisms and functions. *Nat Rev Mol Cell Biol* 12: 773 – 786

Janson ME, Dogterom M (2004) A bending mode analysis for growing microtubules: evidence for a velocity-dependent rigidity. *Biophys J* 87: 2723 – 2736

Janson ME, de Dood ME, Dogterom M (2003) Dynamic instability of microtubules is regulated by force. *J Cell Biol* 161: 1029 – 1034

Jaqaman K, Loerke D, Mettlen M, Kuwata H, Grinstein S, Schmid SL, Danuser G (2008) Robust single-particle tracking in live-cell time-lapse sequences. *Nat Methods* 5: 695 – 702

Jha R, Roostalu J, Cade NI, Trokter M, Surrey T (2017) Combinatorial regulation of the balance between dynein microtubule end accumulation and initiation of directed motility. *EMBO J* 36: 3387 – 3404

Kalman RE (1960) A new approach to linear filtering and prediction problems. *J Basic Eng* 82: 35 – 45

Kamath RS, Ahringer J (2003) Genome-wide RNAi screening in *Caenorhabditis elegans*. *Methods* 30: 313 – 321

Kervrann C, Sorzano CÓS, Acton ST, Olivo-Marin J-C, Unser M (2016) A guided tour of selected image processing and analysis methods for fluorescence and electron microscopy. *IEEE J Sel Top Signal Process* 10: 6 – 30

Kim T, Moyle MW, Lara-Gonzalez P, De Groot C, Oegema K, Desai A (2015) Kinetochore-localized BUB-1/BUB-3 complex promotes anaphase onset in *C. elegans*. *J Cell Biol* 209: 507 – 517

Kimura A, Onami S (2005) Computer simulations and image processing reveal length-dependent pulling force as the primary mechanism for *C. elegans* male pronuclear migration. *Dev Cell* 8: 765 – 775

Kimura A, Onami S (2007) Local cortical pulling-force repression switches centrosomal centration and posterior displacement in *C. elegans*. *J Cell Biol* 179: 1347 – 1354

Kimura K, Kimura A (2011) Intracellular organelles mediate cytoplasmic pulling force for centrosome centration in the *Caenorhabditis elegans* early embryo. *Proc Natl Acad Sci USA* 108: 137 – 142

Kotak S (2019) Mechanisms of spindle positioning: lessons from worms and mammalian cells. *Biomolecules* 9: 80

Kozlowski C, Srayko M, Nedelec F (2007) Cortical microtubule contacts position the spindle in *C. elegans* embryos. *Cell* 129: 499 – 510

Krueger LE, Wu J-C, Tsou M-FB, Rose LS (2010) LET-99 inhibits lateral posterior pulling forces during asymmetric spindle elongation in *C. elegans* embryos. *J Cell Biol* 189: 481 – 495

Kunda P, Baum B (2009) The actin cytoskeleton in spindle assembly and positioning. *Trends Cell Biol* 19: 174 – 179

Kunda P, Pelling AE, Liu T, Baum B (2008) Moesin controls cortical rigidity, cell rounding, and spindle morphogenesis during mitosis. *Curr Biol* 18: 91 – 101

Kurup N, Li Y, Goncharov A, Jin Y (2018) Intermediate filament accumulation can stabilize microtubules in *Caenorhabditis elegans* motor neurons. *Proc Natl Acad Sci USA* 115: 3114 – 3119

Laan L, Pavin N, Husson J, Romet-Lemonne G, van Duijn M, López MP, Vale RD, Jülicher F, Reck-Peterson SL, Dogterom M (2012a) Cortical dynein controls microtubule dynamics to generate pulling forces that position microtubule asters. *Cell* 148: 502 – 514

Laan L, Roth S, Dogterom M (2012b) End-on microtubule-dynein interactions and pulling-based positioning of microtubule organizing centers. *Cell Cycle* 11: 3750 – 3757

Labbé JC, Maddox PS, Salmon E, Goldstein B (2003) PAR proteins regulate microtubule dynamics at the cell cortex in *C. elegans*. *Curr Biol* 13: 707 – 714

Labbé J-C, McCarthy EK, Goldstein B (2004) The forces that position a mitotic spindle asymmetrically are tethered until after the time of spindle assembly. *J Cell Biol* 167: 245 – 256

Lacroix B, Ryan J, Dumont J, Maddox PS, Maddox AS (2016) Identification of microtubule growth deceleration and its regulation by conserved and novel proteins. *Mol Biol Cell* 27: 1479 – 1487

Lacroix B, Van Dijk J, Gold ND, Guizetti J, Aldrian-Herrada G, Rogowski K, Gerlich DW, Janke C (2010) Tubulin polyglutamylation stimulates spastin-mediated microtubule severing. *J Cell Biol* 189: 945 – 954

Laurence TA, Chromy BA (2010) Efficient maximum likelihood estimator fitting of histograms. *Nat Methods* 7: 338 – 339

Lee KCB, Siegel J, Webb SED, Lévêque-Fort S, Cole MJ, Jones R, Dowling K, Lever MJ, French PMW (2001) Application of the stretched exponential function to fluorescence lifetime imaging. *Biophys J* 81: 1265 – 1274

Leung CL, Sun D, Zheng M, Knowles DR, Liem RKH (1999) Microtubule actin cross-linking factor (Macf): a hybrid of dystonin and dystrophin that can interact with the actin and microtubule cytoskeletons. *J Cell Biol* 147: 1275 – 1286

Lewellyn L, Dumont J, Desai A, Oegema K (2010) Analyzing the effects of delaying aster separation on furrow formation during cytokinesis in the *Caenorhabditis elegans* embryo. *Mol Biol Cell* 21: 50 – 62

Li S, Besson S, Blackburn C, Carroll M, Ferguson RK, Flynn H, Gillen K, Leigh R, Lindner D, Linkert M *et al* (2016) Metadata management for high content screening in OMERO. *Methods* 96: 27 – 32

Maton G, Edwards F, Lacroix B, Stefanutti M, Laband K, Lieury T, Kim T, Espeut J, Canman JC, Dumont J (2015) Kinetochore components are required for central spindle assembly. *Nat Cell Biol* 17: 697 – 705

Maus M, Cotlet M, Hofkens J, Gensch T, De Schryver FC, Schaffer J, Seidel CAM (2001) An experimental comparison of the maximum likelihood estimation and nonlinear least-squares fluorescence lifetime analysis of single molecules. *Anal Chem* 73: 2078 – 2086

McCarthy Campbell EK, Werts AD, Goldstein B (2009) A cell cycle timer for asymmetric spindle positioning. *PLoS Biol* 7: e1000088

McNally FJ (2013) Mechanisms of spindle positioning. *J Cell Biol* 200: 131 – 140

Mitchison T, Kirschner M (1984) Dynamic instability of microtubule growth. *Nature* 312: 237 – 242

Morin X, Bellaïche Y (2011) Mitotic spindle orientation in asymmetric and symmetric cell divisions during animal development. *Dev Cell* 21: 102 – 119

Motegi F, Sugimoto A (2006) Sequential functioning of the ECT-2 RhoGEF, RHO-1 and CDC-42 establishes cell polarity in *Caenorhabditis elegans* embryos. *Nat Cell Biol* 8: 978 – 985

Motegi F, Velarde NV, Piano F, Sugimoto A (2006) Two phases of astral microtubule activity during cytokinesis in *C. elegans* embryos. *Dev Cell* 10: 509 – 520

Munro E, Nance J, Priess JR (2004) Cortical flows powered by asymmetrical contraction transport PAR proteins to establish and maintain anterior-posterior polarity in the early *C. elegans* embryo. *Dev Cell* 7: 413 – 424

Needleman DJ, Groen A, Ohi R, Maresca T, Mirny L, Mitchison T (2010) Fast microtubule dynamics in meiotic spindles measured by single molecule imaging: evidence that the spindle environment does not stabilize microtubules. *Mol Biol Cell* 21: 323 – 333

Neumüller RA, Knoblich JA (2009) Dividing cellular asymmetry: asymmetric cell division and its implications for stem cells and cancer. *Genes Dev* 23: 2675 – 2699

Nguyen-Ngoc T, Afshar K, Gonczy P (2007) Coupling of cortical dynein and G [alpha] proteins mediates spindle positioning in *Caenorhabditis elegans*. *Nat Cell Biol* 9: 1294 – 1302

Nishimura G, Tamura M (2005) Artefacts in the analysis of temporal response functions measured by photon counting. *Phys Med Biol* 50: 1327 – 1342

Nørrelykke SF, Flyvbjerg H (2010) Power spectrum analysis with least-squares fitting: amplitude bias and its elimination, with application to optical tweezers and atomic force microscope cantilevers. *Rev Sci Instrum* 81: 75103

Oegema K, Desai A, Rybina S, Kirkham M, Hyman AA (2001) Functional analysis of kinetochore assembly in *Caenorhabditis elegans*. *J Cell Biol* 153: 1209 – 1226

Olson SK, Greenan G, Desai A, Müller-Reichert T, Oegema K (2012) Hierarchical assembly of the eggshell and permeability barrier in *C. elegans*. *J Cell Biol* 198: 731 – 748

O'Rourke SM, Christensen SN, Bowerman B (2010) *Caenorhabditis elegans* EFA-6 limits microtubule growth at the cell cortex. *Nat Cell Biol* 12: 1235 – 1241

O'Rourke SM, Dorfman MD, Carter JC, Bowerman B (2007) Dynein modifiers in *C. elegans*: light chains suppress conditional heavy chain mutants. *PLoS Genet* 3: e128

Panbianco C, Weinkove D, Zanin E, Jones D, Divecha N, Gotta M, Ahringer J (2008) A casein kinase 1 and PAR proteins regulate asymmetry of a PIP2 synthesis enzyme for asymmetric spindle positioning. *Dev Cell* 15: 198 – 208

Park DH, Rose LS (2008) Dynamic localization of LIN-5 and GPR-1/2 to cortical force generation domains during spindle positioning. *Dev Biol* 315: 42 – 54

Pavin N, Laan L, Ma R, Dogterom M, Jülicher F (2012) Positioning of microtubule organizing centers by cortical pushing and pulling forces. *New J Phys* 14: 105025

Pécréaux J, Redemann S, Alayan Z, Mercat B, Pastezeur S, Garzon-Coral C, Hyman Anthony A, Howard J (2016) The mitotic spindle in the one-cell *C. elegans* embryo is positioned with high precision and stability. *Biophys J* 111: 1773 – 1784

Pécréaux J, Röper J-C, Kruse K, Jülicher F, Hyman AA, Grill SW, Howard J (2006a) Spindle oscillations during asymmetric cell division require a threshold number of active cortical force generators. *Curr Biol* 16: 2111 – 2122

Pécréaux J, Zimmer C, Olivo-Marin J-C (2006b) Biophysical active contours for cell tracking I: Tension and bending, Image Processing, 2006 IEEE International Conference on. IEEE, pp. 1949 – 1952

Peris L, Thery M, Fauré J, Saoudi Y, Lafanechère L, Chilton JK, Gordon-Weeks P, Galjart N, Bornens M, Wordeman L (2006) Tubulin tyrosination is a major factor affecting the recruitment of CAP-Gly proteins at microtubule plus ends. *J Cell Biol* 174: 839 – 849

Peris L, Wagenbach M, Lafanechère L, Brocard J, Moore AT, Kozielski F, Job D, Wordeman L, Andrieux A (2009) Motor-dependent microtubule disassembly driven by tubulin tyrosination. *J Cell Biol* 185: 1159 – 1166

Perlson E, Hendricks AG, Lazarus JE, Ben-Yaakov K, Gradus T, Tokito M, Holzbaur ELF (2013) Dynein interacts with the neural cell adhesion molecule (NCAM180) to tether dynamic microtubules and maintain synaptic density in cortical neurons. *J Biol Chem* 288: 27812 – 27824

Praitis V, Casey E, Collar D, Austin J (2001) Creation of low-copy integrated transgenic lines in *Caenorhabditis elegans*. *Genetics* 157: 1217 – 1226

Preciado Lopez M, Huber F, Grigoriev I, Steinmetz MO, Akhmanova A, Dogterom M, Koenderink GH (2014a) In vitro reconstitution of dynamic microtubules interacting with actin filament networks. *Methods Enzymol* 540: 301 – 320

Preciado Lopez M, Huber F, Grigoriev I, Steinmetz MO, Akhmanova A, Koenderink GH, Dogterom M (2014b) Actin-microtubule coordination at growing microtubule ends. *Nat Commun* 5: 4778

Redemann S, Baumgart J, Lindow N, Shelley M, Nazockdast E, Kratz A, Prohaska S, Brugués J, Fürthauer S, Müller-Reichert T (2017) *C. elegans* chromosomes connect to centrosomes by anchoring into the spindle network. *Nat Commun* 8: 15288

Redemann S, Pécréaux J, Goehring NW, Khairy K, Stelzer EHK, Hyman AA, Howard J (2010) Membrane invaginations reveal cortical sites that pull on mitotic spindles in one-cell *C. elegans* embryos. *PLoS One* 5: e12301

Reymann A-C, Staniscia F, Erzberger A, Salbreux G, Grill SW (2016) Cortical flow aligns actin filaments to form a furrow. *Elife* 5: e17807

Riche S, Zouak M, Argoul F, Arneodo A, Pécréaux J, Delattre M (2013) Evolutionary comparisons reveal a positional switch for spindle pole oscillations in *Caenorhabditis* embryos. *J Cell Biol* 201: 653 – 662

Riddle DLBT, Meyer BJ, Priess JR (1997) *C. elegans II*. New York, NY: Cold Spring Harbor Laboratory Press

Rodriguez-Garcia R, Chesneau L, Pastezeur S, Roul J, Tramier M, Pécréaux J (2018) The polarity-induced force imbalance in *Caenorhabditis elegans* embryos is caused by asymmetric binding rates of dynein to the cortex. *Mol Biol Cell* 29: 3093 – 3104

Sallé J, Xie J, Ershov D, Lacassin M, Dmitrieff S, Minc N (2018) Asymmetric division through a reduction of microtubule centering forces. *J Cell Biol* 218: 771 – 782

Schmidt DJ, Rose DJ, Saxton WM, Strome S (2005) Functional analysis of cytoplasmic dynein heavy chain in *Caenorhabditis elegans* with fast-acting temperature-sensitive mutations. *Mol Biol Cell* 16: 1200 – 1212

Schmidt R, Fielmich LE, Grigoriev I, Katrukha EA, Akhmanova A, van den Heuvel S (2017) Two populations of cytoplasmic dynein contribute to spindle positioning in *C. elegans* embryos. *J Cell Biol* 216: 2777 – 2793

Schubert CM, Lin R, De Vries CJ, Plasterk RHA, Priess JR (2000) MEX-5 and MEX-6 function to establish soma/germline asymmetry in early *C. elegans* embryos. *Mol Cell* 5: 671 – 682

Schulze E, Asai DJ, Bulinski JC, Kirschner M (1987) Posttranslational modification and microtubule stability. *J Cell Biol* 105: 2167 – 2177

Schwarz G (1978) Estimating the dimension of a model. *Ann Stat* 6: 461 – 464

Severson AF, Bowerman B (2003) Myosin and the PAR proteins polarize microfilament-dependent forces that shape and position mitotic spindles in *Caenorhabditis elegans*. *J Cell Biol* 161: 21 – 26

Shinar T, Mana M, Piano F, Shelley MJ (2011) A model of cytoplasmically driven microtubule-based motion in the single-celled *Caenorhabditis elegans* embryo. *Proc Natl Acad Sci USA* 108: 10508 – 10513

Siegel J, Lee KB, Webb SE, Leveque-Fort S, Cole MJ, Jones R, Dowling K, French PM, Lever M (2001) Application of the stretched exponential function to fluorescence lifetime imaging of biological tissue, European Conference on Biomedical Optics. International Society for Optics and Photonics, pp. 99 – 107

Srayko M, Kaya A, Stamford J, Hyman AA (2005) Identification and characterization of factors required for microtubule growth and nucleation in the early *C. elegans* embryo. *Dev Cell* 9: 223 – 236

Srayko M, Quintin S, Schwager A, Hyman AA (2003) *Caenorhabditis elegans* TAC-1 and ZYG-9 form a complex that is essential for long astral and spindle microtubules. *Curr Biol* 13: 1506

Srinivasan DG, Fisk RM, Xu H, Van Den Heuvel S (2003) A complex of LIN-5 and GPR proteins regulates G protein signaling and spindle function in *C. elegans*. *Science's STKE* 17: 1225

Strome S, Wood WB (1983) Generation of asymmetry and segregation of germ-line granules in early *C. elegans* embryos. *Cell* 35: 15 – 25

Sugioka K, Fielmich L-E, Mizumoto K, Bowerman B, van den Heuvel S, Kimura A, Sawa H (2018) Tumor suppressor APC is an attenuator of spindle-pulling forces during *C. elegans* asymmetric cell division. *Proc Natl Acad Sci USA* 115: E954 – E963

Tinevez JY, Dragavon J, Baba-Aissa L, Roux P, Perret E, Canivet A, Galy V, Shorte S (2012) A quantitative method for measuring phototoxicity of a live cell imaging microscope. *Methods Enzymol* 506: 291 – 309

Tolic-Nørrelykke IM, Sacconi L, Thon G, Pavone FS (2004) Positioning and elongation of the fission yeast spindle by microtubule-based pushing. *Curr Biol* 14: 1181 – 1186

Tran P, Marsh L, Doye V, Inoue S, Chang F (2001) A mechanism for nuclear positioning in fission yeast based on microtubule pushing. *J Cell Biol* 153: 397 – 412

Tsou MFB, Hayashi A, DeBella LR, McGrath G, Rose LS (2002) LET-99 determines spindle position and is asymmetrically enriched in response to PAR polarity cues in *C. elegans* embryos. *Development* 129: 4469 – 4481

Tsou M-FB, Hayashi A, Rose LS (2003) LET-99 opposes Gα/GPR signaling to generate asymmetry for spindle positioning in response to PAR and MES-1/SRC-1 signaling. *Development* 130: 5717 – 5730

Turton DA, Reid GD, Beddard GS (2003) Accurate analysis of fluorescence decays from single molecules in photon counting experiments. *Anal Chem* 75: 4182 – 4187

Vieland VJ, Hodge SE (1998) Statistical evidence: a likelihood paradigm. *The American Journal of Human Genetics* 63: 283 – 289

van der Voet M, Berends CW, Perreault A, Nguyen-Ngoc T, Gönczy P, Vidal M, Boxem M, van den Heuvel S (2009) NuMA-related LIN-5, ASPM-1, calmodulin and dynein promote meiotic spindle rotation independently of cortical LIN-5/GPR/Gα. *Nat Cell Biol* 11: 269 – 277

Webster DR, Gundersen GG, Bulinski JC, Borisy GG (1987a) Assembly and turnover of detyrosinated tubulin in vivo. *J Cell Biol* 105: 265 – 276

Webster DR, Gundersen GG, Bulinski JC, Borisy GG (1987b) Differential turnover of tyrosinated and detyrosinated microtubules. *Proc Natl Acad Sci USA* 84: 9040 – 9044

Wloga D, Gaertig J (2010) Post-translational modifications of microtubules. *J Cell Sci* 123: 3447 – 3455

Wright AJ, Hunter CP (2003) Mutations in a β-tubulin disrupt spindle orientation and microtubule dynamics in the early *Caenorhabditis elegans* embryo. *Mol Biol Cell* 14: 4512 – 4525

Wu H-Y, Nazockdast E, Shelley MJ, Needleman DJ (2017) Forces positioning the mitotic spindle: theories, and now experiments. *BioEssays* 39: 1600212

Wu JC, Rose LS (2007) PAR-3 and PAR-1 inhibit LET-99 localization to generate a cortical band important for spindle positioning in *Caenorhabditis elegans* embryos. *Mol Biol Cell* 18: 4470 – 4482

Wühr M, Dumont S, Groen AC, Needleman DJ, Mitchison TJ (2009) How does a millimeter-sized cell find its center? *Cell Cycle* 8: 1115 – 1121

Yogev S, Maeder CI, Cooper R, Horowitz M, Hendricks AG, Shen K (2017) Local inhibition of microtubule dynamics by dynein is required for neuronal cargo distribution. *Nat Commun* 8: 15063

Zanic M, Stear JH, Hyman AA, Howard J (2009) EB1 recognizes the nucleotide state of tubulin in the microtubule lattice. *PLoS One* 4: e7585

Zhang S, Banerjee D, Kuhn JR (2011) Isolation and culture of larval cells from *C. elegans*. *PLoS One* 6: e19505

Zhao T, Graham OS, Raposo A, St Johnston D (2012) Growing microtubules push the oocyte nucleus to polarize the *Drosophila* dorsal-ventral axis. *Science* 336: 999 – 1003

Zhu J, Burakov A, Rodionov V, Mogilner A (2010) Finding the cell center by a balance of dynein and myosin pulling and microtubule pushing: a computational study. *Mol Biol Cell* 21: 4418 – 4427

